# Global environmental consequences of 21st century ice sheet melt

Nicholas R. Golledge[1,2*], Elizabeth D. Keller[2], Natalya Gomez[3], Kaitlin A. Naughten[4], Jorge Bernales[5], Luke D. Trusel[6], and Tamsin L. Edwards[7]

[1] Antarctic Research Centre, Victoria University of Wellington, Wellington 6140, New Zealand

[2] GNS Science, Avalon, Lower Hutt 5011, New Zealand

[3] Earth and Planetary Sciences, McGill University, Montreal, Canada

[4] British Antarctic Survey, Cambridge, United Kingdom

[5] MARUM Centre for Marine Environmental Sciences, University of Bremen, Bremen, Germany

[6] Department of Geology, Rowan University, New Jersey, USA

[7] Department of Geography, Kings College, London, United Kingdom

[*]e-mail: nicholas.golledge@vuw.ac.nz

**Government policies currently commit us to 3–4°C surface warming above pre-industrial levels by 2100 CE, which will lead to enhanced ice-sheet melt. Explicit representation of ice sheet discharge was not included in Coupled Model Intercomparison Project Phase 5, so climate impacts arising from this melt are currently not captured in the simulations most commonly used to inform governmental policy. Here we show, using Greenland and Antarctic ice-sheet simulations constrained by satellite-based measurements of recent ice mass change, that increasing meltwater from Greenland will lead to substantial slowing of the Atlantic overturning circulation, and meltwater from Antarctica will trap warm water below the sea surface in a way that creates a positive feedback, increasing Antarctic ice loss. In our simulations, future ice-sheet melt enhances global temperature variability and contributes up to 25 cm to sea level by 2100 CE. Uncertainties in the way that future ice dynamic changes are modelled still remain, however, underlining the need for continued observations and comprehensive multi-model assessments.**

**Introduction** Mass loss from the Antarctic[1,2] and Greenland[2,3] ice sheets and from mountain glaciers[4] is accelerating[5], primarily as a consequence of rising atmospheric and oceanic temperatures. This ice loss contributes to the recently observed acceleration in global mean sea level rise[6] and may also be linked to weakening of the Atlantic Meridional Overturning Circulation (AMOC)[7,8]. It is likely that global temperatures in 2100 CE will exceed the 2°C target set by the Paris Agreement[9], because even if the pledges made by signatory countries of the Paris Agreement are honoured, simulations indicate a likely increase of 2.6–4.0°C above preindustrial baseline temperatures[10]. The Greenland Ice Sheet (GrIS), the West Antarctic Ice Sheet (WAIS), and the AMOC are all capable of abrupt changes under perturbed climate conditions[11]. Recent research suggests that tipping points in parts of the West Antarctic ice sheet may already have been passed[12,13]. Coastal flooding events in low latitude areas will likely double in frequency

by 2050 if sea level rise (SLR) reaches 0.1–0.2 m above present[14], with less developed small island nations likely to experience the greatest local climate changes if the Paris targets are not met[15]. The consequences of predicted future Earth system changes will therefore be societally and economically significant, but impacts will be spatially variable and the spread of future SLR scenarios remains large due to uncertainties in the processes likely to control future ice-sheet retreat[16]. Even within climatologies consistent with the Paris targets there is a likelihood of at least 0.5 m global mean SLR by 2100[17].

Global mean sea level depends primarily on five key contributors: the Greenland and Antarctic ice sheets, mountain glaciers, land water storage, and ocean thermal expansion. Of these, the ice sheet components represent the greatest sea-level potential and are the most capable of abrupt or non-linear change. Previous 'scenario-based' simulations using dynamical ice sheet models and forced by climate scenarios adopted by the Intergovernmental Panel on Climate Change (IPCC) have forecast a range of possible sea-level contributions by the end of the century[18–21]. To-date, however, no single study has simulated both the Greenland and Antarctic ice sheets at high resolution and in a consistent framework that incorporates time-varying multi-parameter mass balance constraints from satellite-era observational records.

Furthermore, experiments undertaken for Coupled Model Intercomparison Project phase 5 (CMIP5) did not include explicit representation of future ice sheet discharge[22–24]. This means that the climate simulations most commonly employed to inform global policy decisions currently do not account for ice–ocean–atmosphere feedbacks that may arise as a consequence of ice sheet melting.

**Experimental methods and approach** Here we present scenario-based simulations of the Greenland and Antarctic ice sheets at horizontal resolutions of 2.5 km and 5 km respectively, employing a sub-grid scale grounding-line parameterization and a hybrid stress balance

calculation that simultaneously solves flow equations that capture the dynamics of inland ice flow, ice streams, and ice shelves[25]. We drive these experiments with spatially and time-varying monthly and annual climatologies from multi-model ensemble mean outputs of CMIP5, through the period 1860 to 2100 CE. Our coupled ice sheet–ice shelf model employs a basal melt rate calculation derived from inversion of present-day melt rates[26] (see 'Methods') allowing spatially distributed sub-ice shelf melt to be captured realistically. To investigate the consequences of incorporating previously ignored ice–ocean–atmosphere feedbacks, we employ offline coupling between our ice sheet model and an intermediate-complexity climate model with a fully coupled ocean and atmosphere, passing results from one to the other in a series of iterations.

**Results and key findings** Figure 1 illustrates the time evolution of our two simulated ice sheets in the first such iteration. We compare modelled quantities of net mass balance, surface mass balance, basal melt of ice shelves and dynamic (calving) losses against empirical constraints from 23 independent studies whose records collectively span the period 1900–2017, with the most complete coverage occuring since 1980. Although we are not able to constrain all parameters through this entire period, and acknowledging that uncertainties in these quantities are high in some cases (Figure 1**b**), our optimized model parameterization (see 'Methods') allows a close fit to be achieved in nearly all cases.

Using this parameterization we first run a suite of future ice sheet simulations in which we impose climatologies from Representative Concentration Pathway (RCP) 4.5 and 8.5 scenarios. Previous studies have shown that ice–ocean interactions – not captured in CMIP5 simulations – significantly affect ice sheet evolution[27] as well as far-field changes in climate[28]. This occurs primarily as a consequence of a decadal to centennial-scale buoyancy-induced reduction in high-latitude ocean overturning when ice sheet melt forms a freshwater lens over the sur-

face of the ice-sheet proximal ocean. By stratifying the water column, upwelling warm water does not mix with colder surface layers, essentially trapping heat in the subsurface where it can spread laterally and increase melting at glacier grounding lines[29,30]. Our coarse-resolution ocean model might underestimate effects from short-term variability in mixed layer thickness, however, which might also influence ocean temperatures (see 'Methods'). We introduce annual transient freshwater fluxes from our simulated ice sheets into the climate simulations from 2000-2100 CE under RCP 4.5 and 8.5 conditions. Time-evolving fluxes are calculated by assuming all mass changes in the ice sheet result in a net flux of freshwater to the proximal ocean, which by 2100 CE reach maxima of approximately 0.042 and 0.015 Sv for Antarctica and Greenland respectively for RCP 4.5, and 0.160 and 0.018 Sv for Antarctica and Greenland respectively under RCP 8.5. Sub-surface ocean temperature, surface air temperature, and precipitation anomalies arising as a consequence of this meltwater addition (compared to a control with no meltwater addition) are added to the previously employed CMIP5 fields and the ice sheet simulations are repeated.

Figure 2 presents the modelled sea level contributions from the two ice sheets by 2100 CE, under RCP 4.5 and 8.5 conditions both with and without ice–ocean–atmosphere feedbacks. It is clear from these trajectories that the sea level contribution from the Greenland ice sheet is approximately linear with time, increasing in magnitude with stronger forcing. The response of the Antarctic ice sheet is slower in the first decades of the century and accelerates subsequently. Combining these two sources yields a globally-averaged pattern of sea-level rise that exhibits episodic accelerations through the century, with the fastest increase in the rate of sea-level rise occuring 2065-2075 under RCP 8.5 conditions with melt feedback incorporated (Fig. 2**d**).

Simulated changes in ice sheet geometries by 2100 CE under an RCP 8.5 climatology, and incorporating ice–ocean–atmosphere feedbacks, show that in Antarctica (Figure 3**a**), the greatest thickness changes this century occur in the grounded ice of the Amundsen Sea sector of West

Antarctica. This is associated with significant recession of the Thwaites Glacier and neighbouring Pine Island Glacier. Considerable thinning of all the major ice shelves and collapse of Larsen C and many of the Dronning Maud Land ice shelves is also evident. In Greenland (Figure 3**b**) the largest thickness changes take place along the southeast and northwest margins of the ice sheet, with thinning also occurring along lower portions of the Northeast Greenland Ice Stream. To estimate the relative importance of different mass balance components in controlling future evolution of each ice sheet, we compare basin-integrated mass balance over 2070–2100 with that at 1970–2000 CE. We assume that changes in ice thickness represent net mass balance changes, changes in cumulative surface flux reflect surface mass balance, and cumulative sub-ice shelf flux corresponds to basal mass balance. Subtracting the latter two terms from the net change in thickness gives an estimate of dynamic losses, which can be equated with loss due to iceberg calving. Using this approach we see that under RCP 8.5 conditions with melt-feedbacks incorporated, net mass balance by the end of the century decreases in almost all Antarctic and Greenland catchments. Several East Antarctic drainage basins experience increasing precipitation and a weakly positive surface mass balance (Figure 3**a**), but across the majority of West Antarctica and all of Greenland, surface accumulation is reduced. Basal melting of floating ice accounts for a significant proportion of Antarctic mass loss but is negligible for much of Greenland, except in northwest and northeast catchments. In Greenland, dynamic (calving) losses are greatest early in the century, before the reduction in surface mass balance begins to dominate from mid-century onwards (Figure 1**f, h**).

Figure 4 shows the environmental consequences by 2100 of adding meltwater fluxes from our two ice sheet simulations to the adjacent ocean. Our climate model simulates globally significant impacts on (**a**), surface air temperature, (**b**), sea surface temperature, (**c**), subsurface (415 m) ocean temperature, and (**h**) sea surface height. The climate anomalies, calculated from the century-end 30 year mean (2090-2120) to smooth out short-term variability, are solely the

consequence of the addition of ice sheet melt from ice sheet simulations under an RCP 8.5 scenario, compared to a climate simulation in which no melt is added but which is otherwise identical. Radiative forcing is held constant, thus the patterns of thermal anomalies arise entirely from changes in ocean mixing and / or atmospheric circulation. Air temperature anomalies (Figure 4**a**) are strongly differentiated between northern and southern high latitudes. In the north, warming occurs over the Greenland Sea (northeast of Greenland) in the region of Svalbard, and as far north as the North Pole (Extended Data Figure 1**a**). In the southern hemisphere, widespread air surface cooling of $>$2°C and locally up to 4°C is evident at latitudes south of approximately 40° (Extended Data Figure 1**b**). Air temperature anomalies reflect the pattern of changes predicted in surface ocean temperatures (Figure 4**b**), although the latter are of lower magnitude. Ocean temperature changes at 415 m depth (Figure 4**c**) – relevant for Antarctic grounding lines – are negative through much of the Southern Ocean away from Antarctica, but widespread warming occurs in mid to low latitudes and in areas where freshwater fluxes are applied close to the simulated ice sheets. Significantly, a substantial sub-surface warming (0.5–1.0°C) is evident around much of the Antarctic continent, with maxima in the Ross Sea, along the coast of West Antarctica, and the western Antarctic Peninsula (Extended Data Figure 1**a, b**).

Our simulations allow the influence of the meltwater feedback to be isolated but do not incorporate the warming from radiative forcing associated with likely future increases in greenhouse gas emissions. To gauge whether the melt feedback mechanism that we investigate is globally, or only locally, important, we compare the magnitude of our predicted changes with anomalies from CMIP5 data in which emissions forcing is implemented but no meltwater fluxes are included (Extended Data Figure 2). This illustrates that even the modest combined ice sheet discharge volume we predict (less than 0.2 Sv at 2100 CE) is sufficient to modify CMIP5 predicted air and sea surface temperatures by as much as 10% in some areas. These anomalies, as

well as our predicted reduction in global mean air temperature increase of approximately 0.3°C by 2100 CE (Extended Data Figure 2), are very consistent with findings from other scenario-based simulations[31].

Perhaps more immediately impactful than gradual warming is the possibility of enhanced interannual temperature variability, implying more widespread or more frequent terrestrial and marine heatwaves. Such events directly affect ecosystems[32,33] and may contribute to long-term changes in Arctic sea-ice thickness[34]. Our coarse-resolution climate model is unable to fully capture short-term weather events, but can still give an indication of whether or not the inclusion of ice sheet meltwater fluxes in higher-resolution models might significantly affect predicted interannual variability (Methods). Compared to control simulations, the inclusion of ice-sheet melt leads to substantial changes in the amplitude of interannual variability ($>50\%$) across the globe, implying significant disruption to annual to decadal-scale climate patterns (Fig. 4**e–g**).

To predict the spatial pattern of sea-level change during the 21st century we use a global sea level model that includes gravitational self-consistency, Earth rotation, and deformation of a radially varying viscoelastic Earth model (Fig. 4**d** and Extended Data Figure 1**c**). Predicted sea level changes are largest and most spatially variable near the ice sheets, in particular in Antarctica where ice mass changes around the periphery of the ice sheet are also variable. Reduced gravitational attraction and uplift of the solid Earth leads to a shallowing of the oceans in regions of ice loss such as the Amundsen Sea Embayment, and the reverse leads to sea level rise in regions of localised ice gain such as near mountainous areas of the Antarctic Peninsula. Our sea level model predicts that by 2100 CE the largest area of high sea level rise from ice sheet melt ($>$ 0.3 m) should occur in the central Pacific Ocean (Figure 4**d**). Much of the mid to low latitudes also experience sea levels around 0.3 m higher than year 2000 values. When thermosteric effects (calculated in our climate model) arising from meltwater-induced oceanic changes are included, a more complex pattern of sea-level rise emerges (Fig. 4**h** and Extended

Data Figure 1**d**). In this instance, changes in the distribution of ocean heat (primarily at depth; Fig. 4**b, c**) lead to substantial changes in sea surface height in some areas, for example in the open ocean around Antarctica (Extended Data Figure 1**d**). In most areas close to the ice sheet, however, rotational / gravitational effects dominate thermosteric changes.

In the North Atlantic, our simulated pattern of temperature anomalies most likely arises from a GrIS meltwater-driven slowdown of the upper cell of the AMOC (Figure 5**a**). Theoretical analysis and model studies indicate that the AMOC is a highly non-linear system that is sensitive to changes in freshwater forcing[35]. Specifically, gradual increases in freshwater bring AMOC strength to a bifurcation point ('saddle node') beyond which no positive stable state is possible and overturning reduces to near zero[35,36]. Recent research has identified a measureable slowdown since pre-industrial times[7,8] and simulations of future changes predict continued weakening, and potential collapse, under unmitigated emissions scenarios[37]. Although our Greenland-derived meltwater fluxes are too low (c. 0.018 Sv under RCP 8.5 with melt feedback) to trigger a collapse of the overturning circulation this century, we nonetheless see a substantial reduction in strength by 2100 CE. In our experiments a gradual slowing in the first half of the century steepens after 2050, leading to a reduction in AMOC strength of 3 to 4 Sv (approximately 15%) over 50 years. This occurs purely as a consequence of the imposed meltwater fluxes and so would presumably add to any weakening from future climate forcing. The lower (counter-clockwise) cell of the AMOC is weaker and responds more slowly, with changes in this instance being forced primarily by Antarctic meltwater (Figure 5**b**). Since current climate models are thought to overestimate the stability of the AMOC[38], it is possible that future ice-sheet meltwater fluxes may play an even more important role than we predict here. Simulations extended to 500 years but without the second iteration of meltwater feedback show an abrupt recovery of AMOC after approximately 300 years (Figure 5**a, b**), in agreement with other studies[39].

**Discussion** The results described above arise from an experimental set-up that 1) is underpinned by time-varying multi-parameter present-day measurements (Figure 1); 2) predicts 21st century ice sheet mass loss in areas where recent thinning has been greatest (Figure 3); and 3) also allows more extreme Antarctic scenarios such as warm interglacial conditions of the early to mid Pliocene to be reproduced (Extended Data Figure 3). In addition, by employing a parameterisation that includes sub-grid melting at glacier grounding lines (see 'Methods') our model produces a sea level contribution from the AIS of 0.14 m by 2100 CE, comparing favourably with the mode (0.15 m, 90% probability interval 0.09 to 0.39 m) for the same scenario derived from a reanalysis of previous simulations[21] in which marine ice cliff instability is excluded[40]. Further, the timing of a positive Antarctic sea-level contribution is almost identical in both our study and the new reanalysis[40], both identifying emergence of a clear signal during the middle of the century.

In our simulation of the GrIS, however we find it necessary to impose two time-varying modifications in order to obtain good fit to observational constraints. From 2000 to 2025 CE we gradually reduce the snowpack refreezing coefficient in our model, such that the surface mass balance trajectory is well captured. This modification is based on prior work identifying that a reduction in refreezing has already taken place in outlying Greenlandic icefields[41] as well as the main ice sheet[42] and is expected to reduce further in the future as the area of bare ice increases[43]. Even with the surface mass balance well represented, fitting to overall net mass balance constraints requires further modification of model parameters. Observations suggest that recent warm water incursions in certain fjords or increased meltwater at the ice sheet bed may be responsible for increased dynamic thinning[44,45]. Although we have no robust way to constrain short-term spatially-variable ocean warming anomalies, by applying a tapered reduction of the basal traction coefficient (reaching a maximum of -40% relative to its initial value)

through the period 2000–2015 we are able to increase dynamic thinning and so match the observed mass loss profile (see 'Experimental Methods' subsection of the 'Methods' and Extended Data Figure 5**d**). This simple approach preferentially accelerates flow in outlet glaciers, where basal sliding is highest, much as would occur if warmer waters led to thinning of the marine terminus. Different parameterisations lead to different initial trajectories, but are all followed by stabilization. This leads us to concur with previous studies[44,45] that future mass loss from Greenland (especially in the latter half of the century in our RCP 8.5 simulation) will be dictated primarily by declining net surface accumulation (Fig. 3**b**), since retreat of marine-terminating glaciers isolates such margins from ocean-driven melt and is therefore a self-limiting process.

In Antarctica, forecast mass losses arise from increasing ice-shelf basal melt and increased iceberg calving of West Antarctic glaciers. We predict the greatest mass loss in the Amundsen Sea sector, primarily associated with thinning and recession of Thwaites Glacier, as predicted in other studies[46]. Our stabilization scenarios illustrate that, even with ocean temperatures held constant from 2020 and without including the meltwater feedback, the loss of a significant portion of WAIS may already be committed (Extended Data Figure 4) and that the pathway of future greenhouse gas emissions will likely only dictate the magnitude and timing of this committed loss. Our simulations show areas of positive surface mass balance across some drainage basins of the East Antarctic Ice Sheet, in line with modern observations[1,47]. In contrast to previous studies[19,21] we do not see a collapse of the Filchner-Ronne or Ross ice shelves by 2100 CE, even under RCP 8.5 conditions. Our observation-constrained melt model instead predicts widespread and significant thinning, together with increased calving, but very little change in overall extent. We do, however, simulate a loss of Larsen C ice shelf and many of the ice shelves fringing Dronning Maud Land. Our model does not include ice shelf hydrofracture or cliff failure mechanics[21] that might hasten retreat. However, it is our contention that such processes are unlikely to be significant during the current century. This is based on three lines of

evidence: 1) by incorporating ice–ocean–atmosphere feedbacks, our new simulations predict significant atmospheric cooling over mid to high southern latitudes (Extended Data Figure 1**b**), offsetting approximately 0.5 to 3.5°C of the atmospheric warming predicted by CMIP5 models (Extended Data Figure 2**c, d**), reducing melt. 2) Although we do not have data from warmer-than-present conditions, contemporary observations show that surface melt has been a normal component of Antarctic ice shelves in the recent past, without it having led to shelf breakup[48,49]. 3) Simulations of future surface melting across Antarctic ice shelves using both regional climate models such as RACMO2.1 (Ref.[50]) as well as CMIP5 general circulation models[51] predict far lower melt quantities than the simulations of Ref.[21]. If such high melt is necessary to induce continent-wide hydrofracture, use of these other models would imply that more extreme atmospheric warming than predicted for 2100 CE may be necessary to trigger widespread ice shelf collapse.

Regardless of the precise magnitude of future ice sheet discharge, rotational, gravitational, Earth deformational and thermosteric effects mean that sea level rise will most substantially affect mid to low latitude island nations in both hemispheres. Ice–ocean–atmosphere feedbacks simulated in our models suggest that sub-surface ocean warming will increase grounding-line retreat around Antarctica and may enhance basal melting of sea ice in the Arctic[34]. By mid-century in our simulations, meltwater from the Greenland ice sheet significantly disrupts the AMOC, which could exacerbate the recently observed slowing trend[7]. Globally, the inclusion of ice sheet meltwater fluxes in climate simulations appears to result in a complex pattern of atmospheric and oceanic changes that include heightened interannual variability in some areas that could result in more frequent extreme weather events.

[1] IMBIE. Mass balance of the Antarctic Ice Sheet from 1992 to 2017. *Nature* **558**, 219–222 (2018).

[2] Forsberg, R., Sørensen, L., and Simonsen, S. Greenland and Antarctic Ice Sheet mass changes and effects on global sea level. *Surveys of Geophysics* **38**, 89–104 (2017).

[3] Chen, X., Zhang, X., Church, J. A., Watson, C. S., King, M. A., Monselesan, D., Legresy, B., and Harig, C. The increasing rate of global mean sea level rise during 1993–2014. *Nature Climate Change* **7**, 492–495 (2017).

[4] Huss, M. and Hock, R. A new model for global glacier change and sea-level rise. *Frontiers in Earth Science* **3**, 54 (2015).

[5] Bamber, J. L., Westaway, R. M., Marzeion, B., and Wouters, B. The land ice contribution to sea level during the satellite era. *Environmental Research Letters* (2018).

[6] Dieng, H. B., Cazenave, A., Meyssignac, B., and Ablain, M. New estimate of the current rate of sea level rise from a sea level budget approach. *Geophysical Research Letters* **44**, 3744–3751 (2017).

[7] Caesar, L., Rahmstorf, S., Robinson, A., Feulner, G., and Saba, V. Observed fingerprint of a weakening Atlantic Ocean overturning circulation. *Nature* **556**, 191–196 (2018).

[8] Thornalley, D. J. R., Oppo, D. W., Ortega, P., Robson, J. I., Brierley, C. M., Davis, R., Hall, I. R., Moffa-Sanchez, P., Rose, N. L., Spooner, P. T., Yashayaev, I., and Keigwin, L. D. Anomalously weak Labrador Sea convection and Atlantic overturning during the past 150 years. *Nature* **556**, 227–230 (2018).

[9] Raftery, A. E., Zimmer, A., Frierson, D. M. W., Startz, R., and Liu, P. Less than 2°C warming by 2100 unlikely. *Nature Climate Change* **7**, 637 (2017).

[10] Climate Action Tracker. . *https://climateactiontracker.org/* , (Accessed 18th June 2018).

[11] Lenton, T. M., Held, H., Kriegler, E., Hall, J. W., Lucht, W., Rahmstorf, S., and Schellnhuber, H. J. Tipping elements in the earth's climate system. *Proceedings of the National Academy of Sciences* **105**(6), 1786–1793, FEB 12 (2008).

[12] Rignot, E., Mouginot, J., Morlighem, M., Seroussi, H., and Scheuchl, B. Widespread, rapid grounding line retreat of Pine Island, Thwaites, Smith, and Kohler glaciers, West Antarctica, from 1992 to 2011. *Geophysical Research Letters* **41**, 35023509 (2014).

[13] Joughin, I., Smith, B. E., and Medley, B. Marine Ice Sheet Collapse Potentially Under Way for the Thwaites Glacier Basin, West Antarctica. *Science* **344**, 735–738 (2014).

[14] Vitousek, S., Barnard, P. L., Fletcher, C. H., Frazer, N., Erikson, L., and Storlazzi, C. D. Doubling of coastal flooding frequency within decades due to sea-level rise. *Scientific Reports* **7**, 1–9 (2017).

[15] King, A. D. and Harrington, L. J. The inequality of climate change from 1.5 to 2°C of global warming. *Geophysical Research Letters* **45**, 5030–5033 (2018).

[16] Kopp, R. E., DeConto, R. M., Bader, D. A., Hay, C. C., Horton, R. M., Kulp, S., Oppenheimer, M., and Pollard, D. aand Strauss, B. H. Evolving understanding of Antarctic ice-sheet physics and ambiguity in probabilistic sea-level projections. *Earth's Future* **5**, 1–17 (2017).

[17] Jackson, L. P., Grinsted, A., and Jevrejeva, S. 21st century sea-level rise in line with the Paris Accord. *Earth's Future* **6**, 1–17 (2018).

[18] Ritz, C., Edwards, T. L., Durand, G., Payne, A. J., Peyaud, V., and Hindmarsh, R. C. Potential sea-level rise from Antarctic ice-sheet instability constrained by observations. *Nature* **528**, 115–118 (2015).

[19] Golledge, N., Kowalewski, D., Naish, T., Levy, R., Fogwill, C., and Gasson, E. The multi-millennial Antarctic commitment to future sea-level rise. *Nature* **526**, 421–425 (2015).

[20] Vizcaino, M., Mikolajewicz, U., Zieman, F., Rodehacke, C. B., Greve, R., and van den Broeke, M. R. Coupled simulations of Greenland Ice Sheet and climate change up to A.D. 2300. *Geophysical Research Letters* **42**, 3927–3935 (2015).

[21] DeConto, R. and Pollard, D. Contribution of Antarctica to past and future sea-level rise. *Nature* **531**, 591–597 (2016).

[22] Weaver, A. J., Sedlácek, J., Eby, M., Alexander, K., Crespin, E., Fichefet, T., Philippon-Berthier, G., Joos, F., Kawamiya, M., Matsumoto, K., Steinacher, M., Tachiiri, K., Tokos, K., Yoshimori, M., and Zickfeld, K. Stability of the Atlantic meridional overturning circulation: A model intercomparison. *Geophysical Research Letters* **39**, 1–7 (2012).

[23] Collins, M., Knutti, R., Arblaster, J., Dufresne, J. L., Fichefet, T., Friedlingstein, P., Gao, X., Gutowski, W. J., Johns, T., Krinner, G., et al. Long-term Climate Change: Projections, Commitments and Irreversibility. In Climate Change 2013 : The Physical Science Basis. Contribution of Working Group I to the Fifth Assessment Report of the Intergovernmental Panel on Climate Change, Stocker, T., Qin, D., Plattner, G.-K., Tignor, M., Allen, S., Boschung, J., Nauels, A., Xia, Y., Bex, V., and Midgley, P. M., editors, 1029–1136. Cambridge University Press (2013).

[24] Bintanja, R., van Oldenborgh, G. J., and Katsman, C. A. The effect of increased fresh water from Antarctic ice shelves on future trends in Antarctic sea ice. *Annals of Glaciology* **56**, 120–126 (2015).

[25] Bueler, E. and Brown, J. Shallow shelf approximation as a "sliding law" in a thermomechanically coupled ice sheet model. *Journal of Geophysical Research* **114**, F03008 (2009).

[26] Bernales, J., Rogozhina, I., and Thomas, M. Melting and freezing under Antarctic ice shelves from a combination of ice-sheet modelling and observations. *Journal of Glaciology* **63**, 731–744 (2017).

[27] Golledge, N., Menviel, L., Carter, L., Fogwill, C., England, M., Cortese, G., and Levy, R. Antarctic contribution to meltwater pulse 1A from reduced Southern Ocean overturning. *Nature Communications* **(5)**, 1–10 (2014).

[28] Bakker, P., Clark, P. U., Golledge, N. R., Schmittner, A., and Weber, M. E. Centennial-scale Holocene climate variations amplified by Antarctic Ice Sheet discharge. *Nature* **541**, 72–76 (2017).

[29] Menviel, L., Timmermann, A., Timm, O. E., and Mouchet, A. Climate and biogeochemical response to a rapid melting of the West Antarctic Ice Sheet during interglacials and implications for future climate. *Paleoceanography* **25** (2010).

[30] Weber, M., Clark, P., Kuhn, G., Timmermann, A., Sprenk, D., Gladstone, R., Zhang, X., Lohmann, G., Menviel, L., Chikamoto, M., et al. Millennial-scale variability in Antarctic ice-sheet discharge during the last deglaciation. *Nature* **510**, 134–138 (2014).

[31] Bronselaer, B., Winton, M., Griffies, S. M., Hurlin, W. J., Rodgers, K. B., Sergienko, O. V., Stouffer, R. J., and Russell, J. L. Change in future climate due to Antarctic meltwater. *Nature* , 1 (2018).

[32] Frölicher, T. L., Fischer, E. M., and Gruber, N. Marine heatwaves under global warming. *Nature* **560**(7718), 360 (2018).

[33] Ruthrof, K. X., Breshears, D. D., Fontaine, J. B., Froend, R. H., Matusick, G., Kala, J., Miller, B. P., Mitchell, P. J., Wilson, S. K., van Keulen, M., et al. Subcontinental heat wave triggers terrestrial and marine, multi-taxa responses. *Scientific Reports* **8**(1), 13094 (2018).

[34] Hutchings, J. K. and Perovich, D. K. Preconditioning of the 2007 sea-ice melt in the eastern Beaufort Sea, Arctic Ocean. *Annals of Glaciology* **56**, 94–98 (2015).

[35] Rahmstorf, S. Bifurcations of the Atlantic thermohaline circulation in response to changes in the hydrological cycle. *Nature* **378**, 145–149 (1995).

[36] Stommel, H. Thermohaline convection with two stable regimes of flow. *Tellus* **13**, 224–230 (1961).

[37] Bakker, P., Schmittner, A., Lenaerts, J., Abe-Ouchi, A., Bi, D., van den Broeke, M., Chan, W.-L., Hu, A., Beadling, R., Marsland, S., et al. Fate of the Atlantic Meridional Overturning Circulation: Strong decline under continued warming and Greenland melting. *Geophysical Research Letters* **43**(23), 12–252 (2016).

[38] Liu, W., Xie, S.-P., Liu, Z., and Zhu, J. Overlooked possibility of a collapsed Atlantic Meridional Overturning Circulation in warming climate. *Science Advances* **3**, e1601666 (2017).

[39] Rind, D., Schmidt, G. A., Jonas, J., Miller, R., Nazarenko, L., Kelley, M., and Romanski, J. Multi-century instability of the Atlantic Meridional Circulation in rapid warming simulations with GISS ModelE2. *Journal of Geophysical Research* **in press**, https://doi.org/10.1029/2017JD027149 (2018).

[40] Edwards, T. L., Brandon, M., Durand, G., Edwards, N. R., Golledge, N. R., Holden, P. B., Nias, I., Payne, A., Ritz, C., and Wernecke, A. Revisiting Antarctic ice loss due to marine ice cliff instability. *accepted* .

[41] Noël, B., van de Berg, W. J., Lhermitte, S., Wouters, B., Machguth, H., Howat, I., Citterio, M., Moholdt, G., Lenaerts, J. T. M., and van den Broeke, M. R. A tipping point in refreezing accelerates mass loss of Greenland's glaciers and ice caps. *Nature Communications* **8**, 14730 (2017).

[42] Machguth, H., MacFerrin, M., van As, D., Box, J. E., Charalampidis, C., Colgan, W., Fausto, R. S., Meijer, H. A., Mosley-Thompson, E., and van de Wal, R. S. Greenland meltwater storage in firn limited by near-surface ice formation. *Nature Climate Change* **6**, 390–393 (2016).

[43] Fettweis, X., Franco, B., Tedesco, M., van Angelen, J., Lenaerts, J. T. M., van den Broeke, M. R., and Gallée, H. Estimating the Greenland ice sheet surface mass balance contribution to future sea level rise using the regional atmospheric climate model MAR. *The Cryosphere* **7**, 469–489 (2013).

[44] Shannon, S. R., Payne, A. J., Bartholomew, I. D., van den Broeke, M. R., Edwards, T. L., Fettweis, X., and others, . Enhanced basal lubrication and the contribution of the Greenland ice sheet to future sea-level rise. *Proceedings of the National Academy of Sciences* **110**, 14156–14161 (2013).

[45] Fürst, J. J., Goelzer, H., and Huybrechts, P. Ice-dynamic projections of the Greenland ice sheet in response to atmospheric and oceanic warming. *The Cryosphere* **9**, 1039–1062 (2015).

[46] Seroussi, H., Nakayama, Y., Larour, E., Menemenlis, D., Morlighem, M., Rignot, E., and Khazendar, A. Continued retreat of Thwaites Glacier, West Antarctica, controlled by bed topography and ocean circulation. *Geophysical Research Letters* **44**(12), 6191–6199 (2017).

[47] Medley, B., McConnell, J. R., Neumann, T. A., Reijmer, C. H., Chellman, N., Sigl, M., and Kipfstuhl, S. Temperature and snowfall in western Queen Maud Land increasing faster than climate model projections. *Geophysical Research Letters* **45**, 1472–1480 (2018).

[48] Phillips, H. A. Surface meltstreams on the Amery Ice Shelf, East Antarctica. *Annals of Glaciology* **27**, 177–181 (1998).

[49] Bevan, S. L., Luckman, A., Hubbard, B., Kulessa, B., Ashmore, D., Kuiper Munneke, P., O'Leary, M., Booth, A., Sevestre, H., and McGrath, D. Centuries of intense surface melt on Larsen C ice shelf. *The Cryosphere* **11**, 2743–2753 (2017).

[50] Trusel, L. D., Frey, K. E., Das, S. B., Karnauskas, K. B., Kuipers Munneke, P., van Meijgaard, E., and van den Broeke, M. Divergent trajectories of Antarctic surface melt under two twenty-first-century climate scenarios. *Nature Geoscience* **8**, 927–932 (2015).

[51] Bell, R. E., Banwell, A., Trusel, L., and Kingslake, J. Antarctic surface hydrology and impacts on ice sheet mass balance. *Nature Climate Change* **8**, 1044–1052 (2018).

**Extended Data** are linked to the online version of the paper at www.nature.com/nature.

**Acknowledgements** We gratefully acknowledge Kevin Buckley (Victoria University high-performance compute cluster), the Parallel Ice Sheet Model groups at University of Alaska, Fairbanks, the Potsdam Institute for Climate Impact Research, and the CMIP community for making their data openly available. PISM is supported by NASA grants NNX13AM16G and NNX13AK27G. This work was funded by contract VUW1501 to NRG from the Royal Society Te Aparangi, with support from the Antarctic Research Centre, Victoria University of Wellington, and GNS Science through the Ministry for Business, Innovation and Employment contract CO5X1001. JB has been supported by the MAGIC-DML project through DFG SPP 1158 (RO 4262/1-6). LDT acknowledges support from NSF Antarctic Glaciology Program (award 1643733).

**Author contributions** NRG devised and carried out the ice-sheet modelling experiments, EK undertook climate model simulations, and NG performed the sea level calculations. KAN, JB, and LDT provided Antarctic basal and surface melt simulations from regional models. All authors contributed to the development of ideas and writing of the manuscript.

**Author information** Reprints and permissions information is available at www.nature.com/reprints. The authors declare no competing financial interests. Correspondence and requests for materials should be addressed to NRG. (nicholas.golledge@vuw.ac.nz).

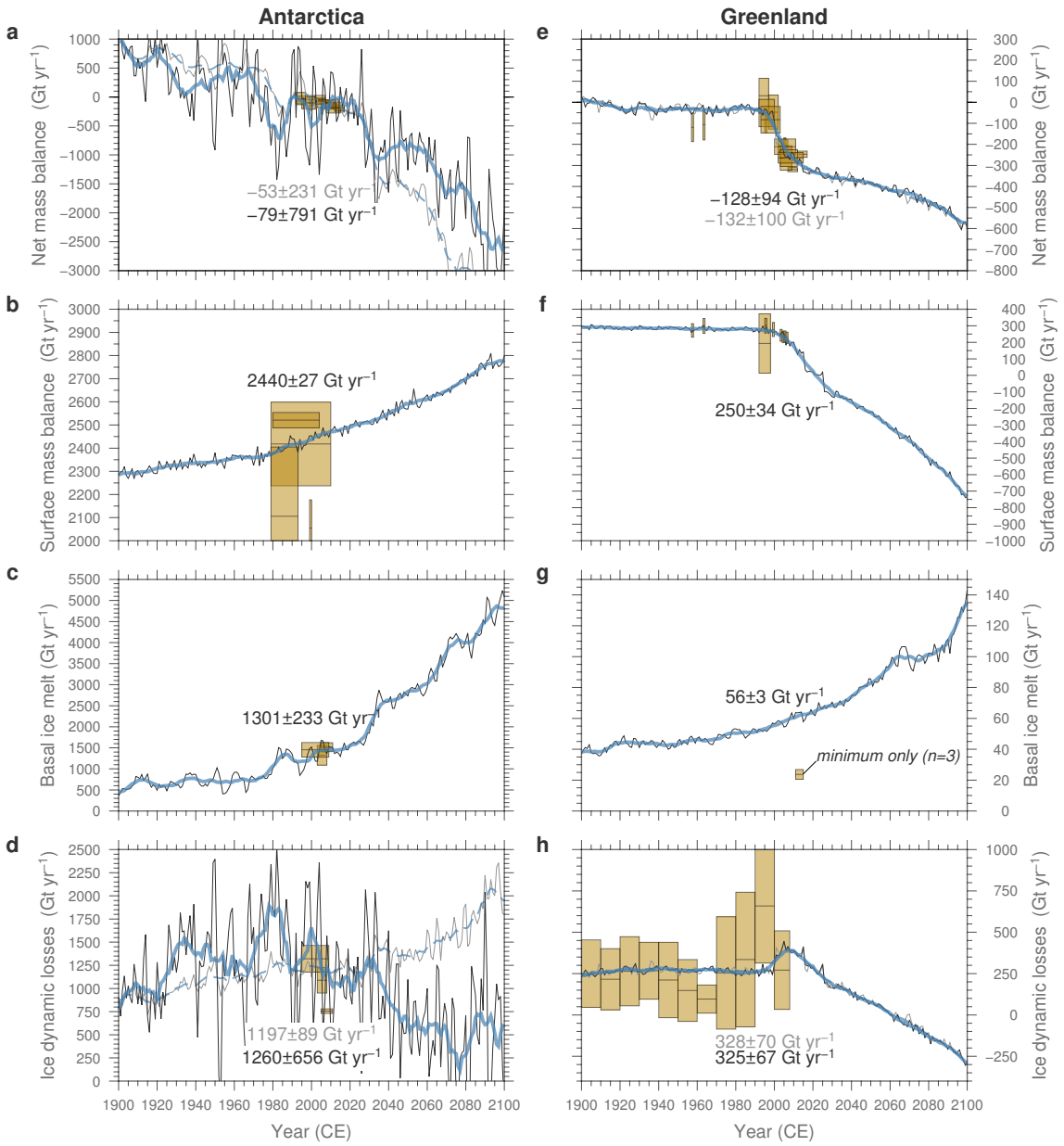


**Figure 1** | **Simulated and observed ice sheet mass balance.** Numerical ice sheet simulation of **a,** net mass balance, **b,** surface mass balance, **c,** basal ice melt, and **d,** ice dynamic (calving) mass loss for the Antarctic ice sheet. Panels **e–h** show the same parameters for the Greenland ice sheet. Negative dynamic losses imply thickening (**h**). Forcing scenario is RCP 8.5; experiments do not include meltwater feedback. Gold boxes show time span ($x$ axis) and uncertainty ($y$ axis) of empirical data values used as targets during parameter optimisation, from sources detailed in Extended Data Tables 1 & 2. Circum-Greenland basal melting is constrained only by one assessment from three glaciers; Greenland calving constraints (**h**) are from data-constrained modelling (Extended Data Table 2). Black lines show annual mass changes for grounded ice only, with 10-yr running mean shown in blue. Grey lines show mass changes for entire ice sheet, including ice shelves. In panels **a, d, e,** and **h** black text denotes 1990–2010 mean for grounded ice, grey text denotes 1990–2010 mean for grounded and floating ice. Plus / minus values indicate one standard deviation of 1990–2010 model range.

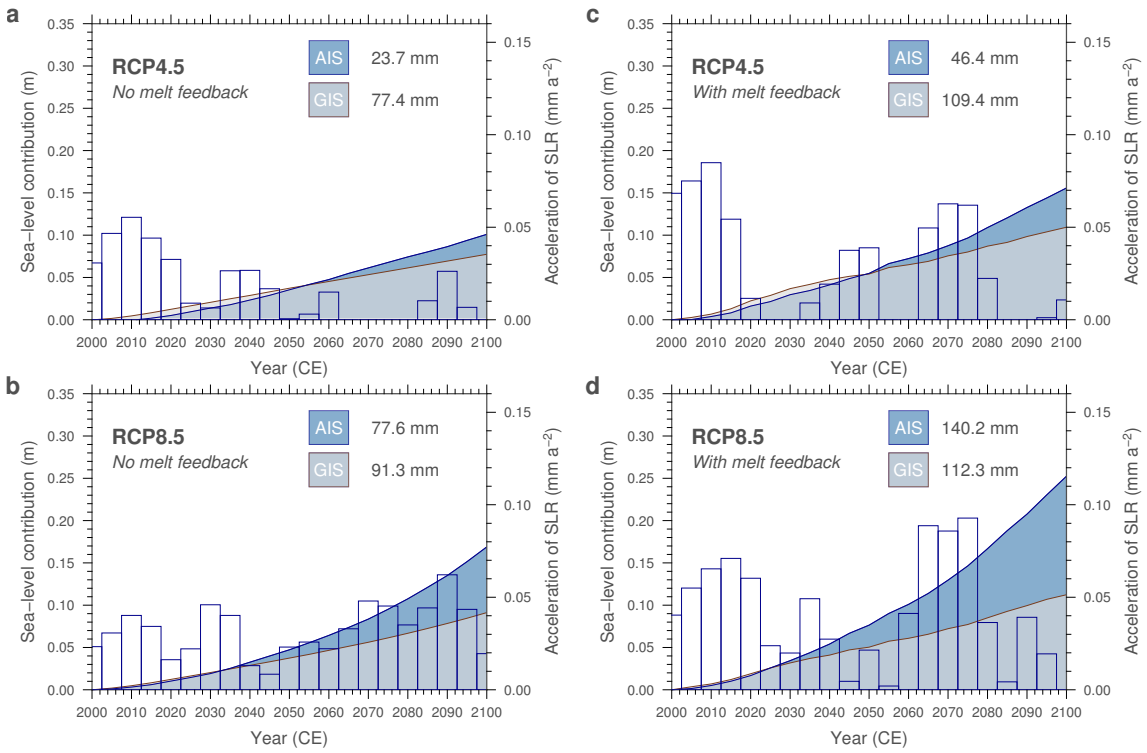


**Figure 2** | **Sea level contributions from Greenland and Antarctica.** Predictions of sea-level equivalent mass loss (metres) from Greenland and Antarctic ice sheets to 2100 CE under RCP 4.5 (**a, c**) and 8.5 (**b, d**) climate trajectories. Column data show rates of acceleration of sea-level rise (positive only, righthand axis) based on combined total of Antarctic and Greenland contributions.

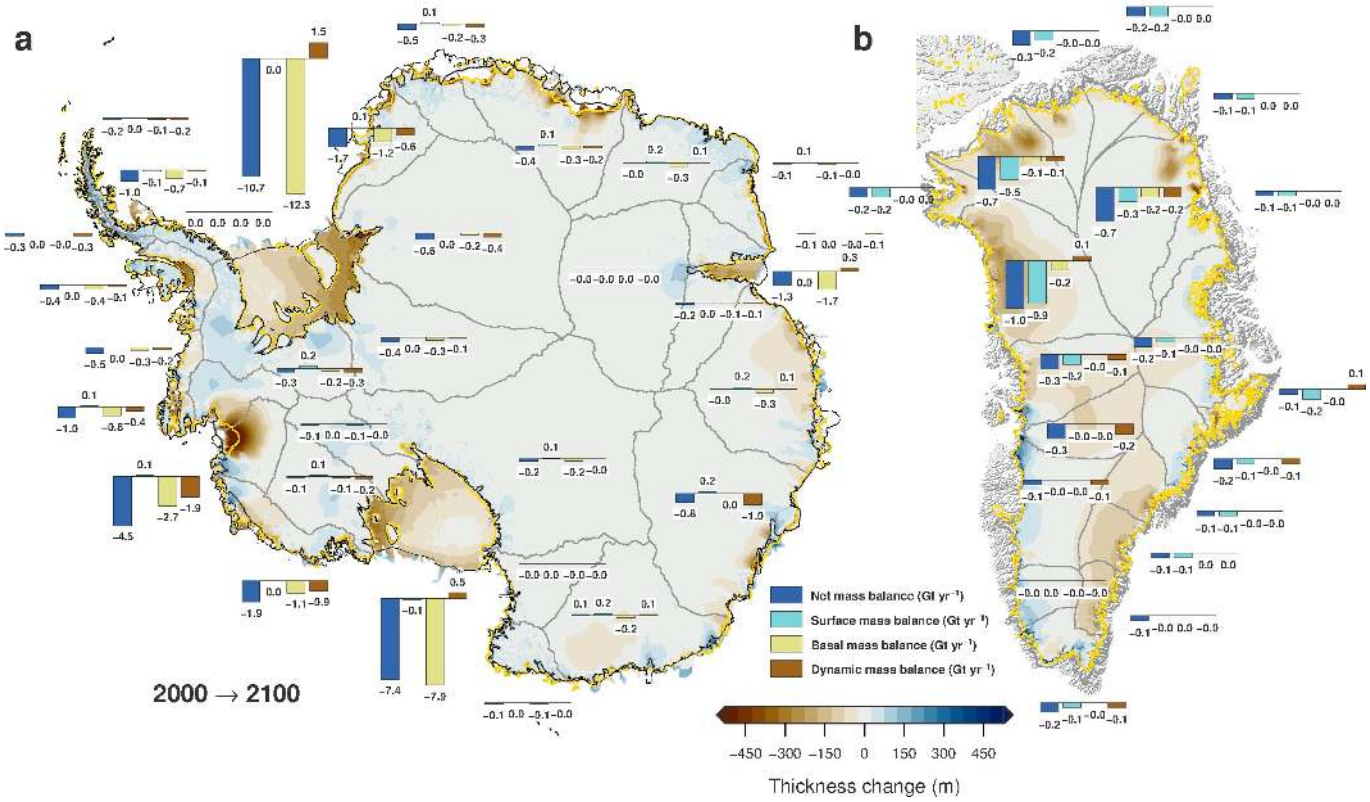


**Figure 3** | **Causes of ice sheet thickness change by 2100.** Simulated patterns of ice sheet thickness change by 2100 CE, compared to 2000 CE, under RCP 8.5 and incorporating ice–ocean–atmosphere feedbacks. Note in **a,** widespread ice shelf thinning and retreat of Thwaites Glacier, and **b,** peripheral thinning around much of the Greenland ice sheet. Bar charts attribute mass change to individual mass balance components, for each ice-sheet catchment (see text). Mass loss values are difference in catchment-integrated annual total at 2100 CE compared to 2000 CE. Grey lines denote ice sheet drainage basin outlines (see 'Methods'). Thin black lines show present-day grounding line and calving line positions (see 'Methods'). Gold lines show modelled grounded ice margins at 2100 CE.

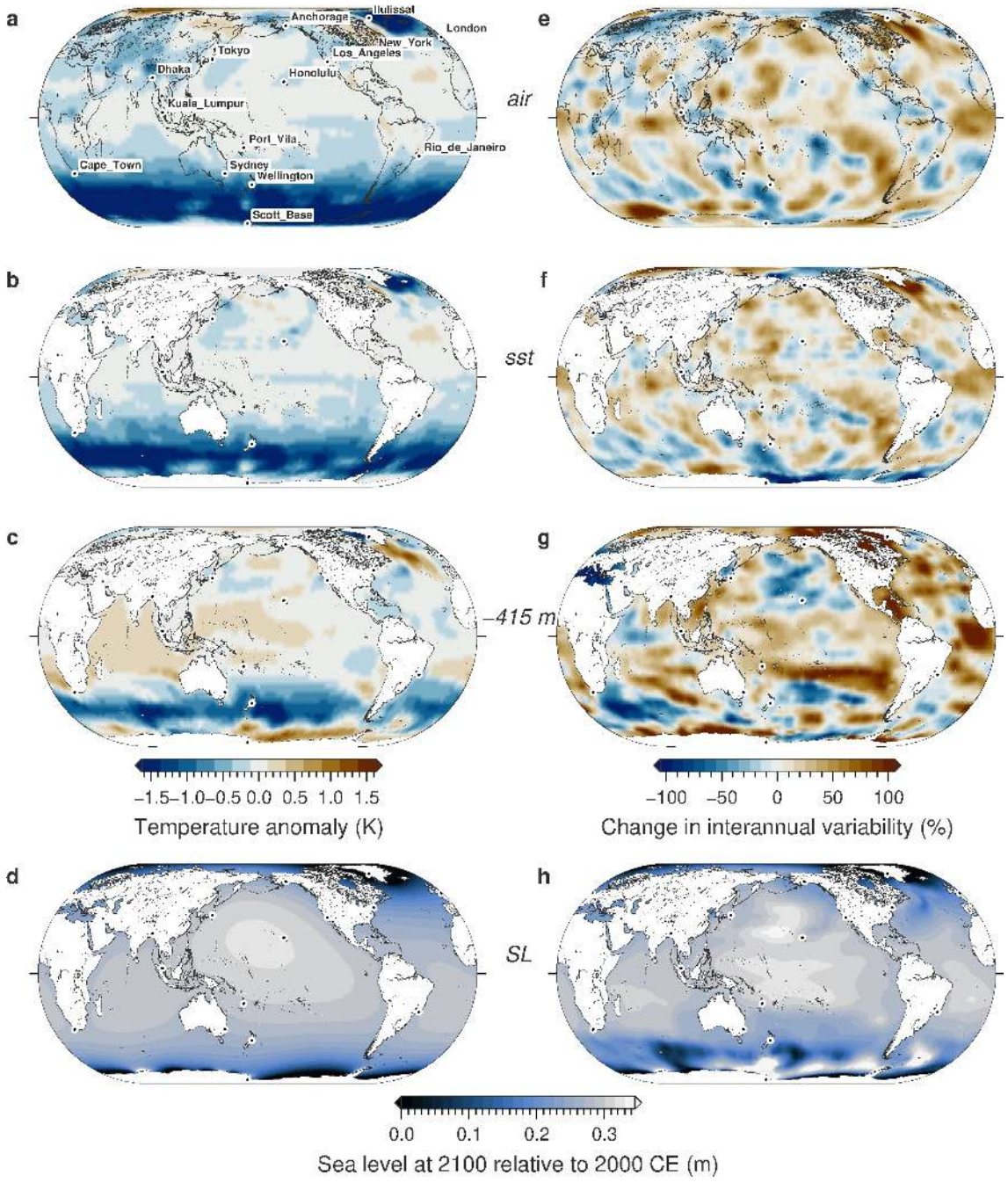


**Figure 4** | **Environmental consequences of 21st century ice sheet meltwater fluxes.** Modelled patterns at 2100 of changes in **a,** air temperature, **b,** sea surface temperature, **c,** subsurface ocean temperature and **d,** sea level, compared to 2000 CE, arising solely from mixing and circulation changes due to input of ice sheet melt simulated under RCP 8.5 conditions with ice–ocean–atmosphere feedbacks. Anomalies are 30-year means to avoid aliasing short-term variability. Note substantial air / ocean surface cooling around Antarctica (**a, b**), and contrasting warming of the subsurface ocean close to coast (**c**). Subsurface warming is also evident in parts of the Arctic. Extended Data Figure 1**a, b** shows polar perspectives. Panels **e–g**, Magnitude of changes in interannual temperature variability by 2100 compared to 2000 due to addition of meltwater. **h,** Sum of modelled sea level rise (**d**) and predicted changes in sea surface height by 2100 arising from thermosteric effects of meltwater input under RCP 8.5 conditions with ice–ocean–atmosphere feedbacks.

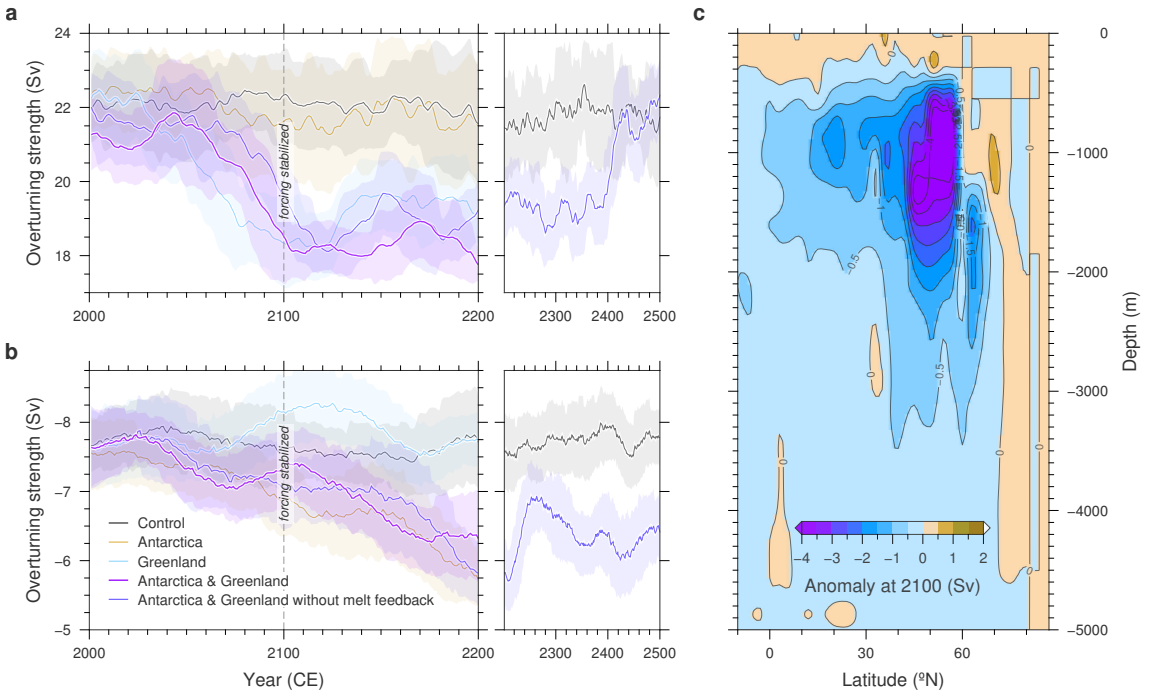


**Figure 5 | Effect of ice sheet melt on Atlantic Meridional Overturning Circulation (AMOC).** Changes in overturning strength of **a,** clockwise and **b,** counter-clockwise components of the AMOC arising in the second climate model iteration that incorporates ice–ocean–atmosphere feedbacks in an ice sheet simulation under RCP 8.5 conditions. Overturning strength is defined as maximum (clockwise) and minimum (counterclockwise) of the meridional overturning streamfunction in the Atlantic Ocean Basin in each year. Effects vary depending on whether added meltwater originates from only the Greenland Ice Sheet (green lines), the Antarctic Ice Sheet (yellow lines), or from both (purple lines). Black lines illustrate a control simulation in which no meltwater is added. Dark blue lines (running to 2500 CE) show results from the first iteration of the ice-sheet and climate simulations, in which ice–ocean–atmosphere feedbacks on the ice sheet are not included. Envelopes represent the evolving 30-year standard deviation of annual data; 30-year running means shown with bold line. **c,** Overturning strength anomalies at 2100 compared to a control run with no ice-sheet meltwater added. Anomalies are 30-year means to avoid aliasing short-term variability. The c. 4 Sv decrease in AMOC strength at 500–1500 m depth takes place over approximately 50 years **(a)**.

## Methods

**The ice sheet model.** We use the Parallel Ice Sheet Model[25,52,53] (PISM) version 0.7.3. PISM is a 'hybrid' ice sheet / shelf model that combines shallow approximations of the flow equations that compute gravitational flow and flow by horizontal stretching. The combined stress balance allows for a consistent treatment of ice sheet flow, from non-sliding grounded ice, to rapidly-sliding grounded ice (ice streams), to floating ice shelves. In common with most continental-scale ice sheet models, PISM incorporates enhancement factors for each component of the stress regime, allowing creep and sliding velocities to be adjusted using simple coefficients. These are model constants, and do not evolve. These enhancement factors enable simulations to be optimized such that modelled behaviour matches observed behaviour. The junction between grounded and floating ice is refined by a sub-grid scale parameterization[54] that smooths both the basal shear stress field and the basal melt. In previous simulations[19,55] we ran duplicate experiments with and without this interpolation of basal melting. Our experimentation revealed that the use of sub-grid melting increases the ability of glacier grounding lines to retreat, leading to faster ice loss. Although the numerical veracity of this approach has been questioned[56], we have previously found little evidence for a grid-size dependency in using this scheme[19] and find instead that it enables simulated mass loss under warmer-than-present palaeoclimate scenarios that is more closely in agreement with proxy reconstructions that when sub-grid melting is omitted[55]. In support of this approach are recent observations confirming that oceanic water intrudes into the grounding zone of marine-terminating Antarctic glaciers in some areas[57], carrying with it heat available for melting of ice. We optimize our model with this scheme and use it in all experiments, but acknowledge that this is an area in which our simulations may introduce uncertainties. To quantify these uncertainties, we ran our control and RCP 8.5 simulations for both ice sheets with and without the sub-grid melt scheme (Extended Data Figure 5**a, b**). These results suggest that whilst the subgrid scheme has little influence in Greenland, our Antarctic runs produce mass loss forecasts approximately 40% lower when subgrid melting is not used. However, our control experiment in these simulations exhibits more substantial deviation from present-day ice volume, suggesting that other parameters may need adjustment in order to accurately capture Antarctic ice sheet evolution *without* use of the subgrid melt scheme. We run our experiments at grid resolutions of 2.5 km (Greenland) and 5 km (Antarctica). By adopting such high resolutions, together with the sub-grid grounding line scheme described above, our model is able to accurately track grounding-line migration[54]. Importantly, we find little evidence of grid dependency in the 5–20 km range, either in previous simulations[19] or in the new experiments presented here (Extended Data Figure 5c).

Mass balance at the ice surface is computed by a positive degree day algorithm that employs degree-day factors of 2 and 4 mm / °C / day for the melting of snow and ice respectively. These very low values are used in conjunction with a positive threshold temperature of 270 K, rather than the usual 273 K, a combination that together has been shown to better reproduce the spatial distribution of surface melting (in Greenland) than achieved with higher melt factors and higher threshold temperature[58]. We use a standard deviation of daily temperature

variability of 2.5 K, and a refreezing coefficient of 0.6 to account for retention of surface melt within the snow or firn, but we vary this coefficient in our Greenland optimization in order to match our predicted surface melt trajectory to empirical constraints. This approach is underpinned by the recognition of recent and forecast changes in refreezing in Greenland[41–43]. Basal mass balance is calculated using a thermodynamic model that reads temperature and salinity values and calculates a melt rate[59]. In our implementation of PISM it is only possible to use a single ocean temperature field, not one that allows depth-varying melt, and thus we have sought to improve the way in which present-day melt fields can be more accurately captured. Specifically, we make a substantial advance over our previous simulations[19] in terms of accurately capturing present-day Antarctic ice shelf basal melt rates by using an empirically-tuned melt simulation[26] to calculate a melt factor. We run an iteration in which we input present-day sea surface temperatures from CMIP5 outputs, and then incrementally adjust our melt factor at each grid point so as to reduce the mismatch between 'observed' melt values (our 'target') and values calculated using the melt scheme (Extended Data Figure 5**c, d**). Our dimensionless coefficient is otherwise unconstrained and may be a source of error when applied to future changes in temperature. However, this simple approach yields predicted melt rates under present-day conditions that match observed values far more closely than melt schemes that are not optimized[19,21]. The consequence of this method is that we correctly simulate the 'cold' cavities of the Ross and Ronne-Filchner ice shelves, whilst also capturing the very high melt rates witnessed in the Amundsen Sea proximal to Thwaites and Pine Island glaciers. We acknowledge, however, that the strength of this approach relies on the relationship between temperature, our melt factor, and the derived melt rate remaining unchanged through time. Since the relationship between water temperature and melt rate is highly variable around Antarctica[60] we do not expect to fully capture all possible scenarios, but aim instead for an improvement over previous simplifications[19,21]. Future ocean circulation changes that are not captured in CMIP5 modelled temperature anomalies may also lead to greater temperature changes in some areas that we are unable to account for with our simple scheme, which may affect our results. An additional simplification in our approach is that, in the absence of a dynamically coupled high-resolution ice-shelf cavity-resolving ocean model we are restricted to simply interpolating our ocean temperature anomalies landward, which will not accurately capture topographic funneling of ocean currents that may focus melt in certain areas[61]. Iceberg calving is calculated in our model using two schemes. In the first, horizontal strain rates are used to derive calving rates, leading to faster calving in areas of fast flow[62]. The second scheme applies a simple but heuristic minimum thickness criterion to ensure that thin floating ice is removed. In our spinup experimentation we employed a minimum thickness value of 200 m, which allowed the major ice shelves to be well-represented. However, to ensure that thinner ice shelves were not automatically lost during our RCP-forced experiments, we reduced this thickness limit to 50 m. In order to reproduce the empirical constraints on calving fluxes as closely as possible (Fig. 1**d, h**), we incrementally adjusted the strain rate exponent ensuring that observed calving front locations were also accurately maintained under present-day conditions.

Present-day conditions For input data to our ice sheet model we use the most up-to-date environmental datasets available. Our ice thickness and bed topography are from BEDMAP2 for Antarctica[63] and from BedMachine v.3 for Greenland[64]. Climatologies come from RACMO2.3[65] (Antarctica) and RACMO2/GR[66] (Greenland). Ocean temperatures are derived for both model domains from CMIP5 simulations of present-day climate, which in Antarctica are combined with the melt factor described above to generate accurate melt rates. Oceanic fields are less well constrained for our Greenland domain since an accurate present-day basal melt map is not available for our inversion. Consequently we use a uniform melt factor and adjust this such that present-day grounding line positions are well captured. Since basal melting plays a less significant role in Greenland compared to Antarctica, we are satisfied that this necessary simplification is justified. Geothermal heat flux maps are taken from Ref.[67] for Antarctica and Ref.[68] for Greenland.

Future climate trajectories For our simulations of ice sheet evolution through the twenty-first century, we use the same CMIP5 multi-model mean climate and ocean fields as employed previously[19], but with the significant difference that in these new experiments we use spatially-varying fields for air temperature, precipitation, and sea surface temperature rather than domain-averaged timeseries. Furthermore, we use monthly resolution surface climate fields for the entire period of our simulations – 1860–2100 – and use annual fields for our ocean temperatures on the basis that ice sheet response is affected primarily by inter-annual variability, rather than seasonal fluctuations that may not be well-captured in the CMIP5 data. As CMIP5 models are particularly prone to biases in the Antarctic region[69–71], care must be taken when selecting models to use as forcing for the ice sheet. Since the CMIP5 multi-model mean has been shown to exhibit the best agreement with present-day atmospheric reanalyses over the Southern Ocean and Antarctica[72], it was chosen to force our simulations. Our focus in these experiments lies in the quantification of ice sheet evolution through the current century. However, we are also interested in long term commitments and to that end we run a series of experiments in which we stabilize climate and ocean forcings either at 2020, 2050, or 2100, and run the simulations under constant forcings through to 2500 CE. We consider only two Representative Concentration Pathways (RCPs), RCP 4.5 and RCP 8.5. The reason for this is that these scenarios effectively bracket the range of global mean temperature increase that current policies and pledges commit us to[10].

**Climate and ocean model.** Climate simulations were performed with the model LOVECLIM v1.3 (Ref.[73]). LOVECLIM (LOch-Vecode-Ecbilt-CLio-agIsm) is an intermediate complexity earth system model with coupled atmosphere, ocean / sea ice, and dynamic vegetation. The atmospheric model ECBilt is a 3-D, spectral T21 model, with 3 vertical levels and 5.6 degree horizontal resolution. The ocean component is CLIO, a free-surface primitive equation model with a 3 x 3 degree horizontal grid resolution and 20 vertical levels, and uses the Gent-McWilliams eddy advection parameterisation[74]. CLIO includes a dynamic-thermodynamic sea ice model. The dynamic vegetation model is VECODE. The ocean carbon cycle component

LOCH was turned off in these simulations since we are primarily interested in the dynamic physical response of the ocean and atmosphere rather than the biogeochemical aspects.

Although this intermediate complexity model is simple in its representation of ocean and atmosphere, it is well-established and is used extensively[27,29,30,73,75–77]. In Chapter 8 of the Fourth Assessment Report of the IPCC[78], comparison of intermediate complexity models (including LOVECLIM) with more sophisticated general circulation models (GCM) revealed that both exhibited similar scatter in their results, and both tended to produce results that, "...agree with observational estimates" (Chapter 8.8.3). Importantly, it was also found that in experiments involving a doubling of atmospheric $CO_2$, the results from intermediate complexity models fell within the range of results from GCMs, implying that their ability to capture climate anomalies was at least on a par with the GCMs investigated in that assessment. Despite this, we interpret our climate fields with caution and focus primarily on the quantification of within-model anomalies (i.e. the difference between a perturbed and a control simulation, using the same model and taking 30-year mean climate states in order to avoid short-term climate variability). This approach should reduce any potential biases inherent in the climate model.

The model was spun up with pre-industrial conditions for 1000 years and then run from the years 1950 to 2000 forced with historical $CO_2$ atmospheric concentrations. The 'control' simulation was continued from this initial state and run for 200 years, holding $CO_2$ constant at the 2000 level (370 ppm). Simulations that used freshwater flux perturbations were started from the same initial state and forced with the same constant $CO_2$ level, but meltwater was added on a yearly basis in the form of a change in the local salinity of the ocean, at a rate prescribed by the output from the ice sheet simulations until 2100. The freshwater flux was then held constant for an additional 100 years at the level reached in the last year of ice sheet output. Freshwater fluxes were added separately for the Greenland (GrIS) and West Antarctic (WAIS) ice sheets, and distributed spatially using a mask in the North Atlantic (GrIS) and from the Ross to the Weddell seas of Antarctica (WAIS). Our Greenland mask applies meltwater to ocean cells in a box spanning 26–43°W, 62–90°N. In Antarctica, the box spans 160–360°E, 64–79°S. Mask extents were defined broadly in order to capture the effects of (unmodelled) iceberg melting. Ice sheet extent and elevation were held fixed at present-day boundaries in all simulations. We ran two additional simulations including only the GrIS (GrIS-only) and WAIS (WAIS-only) meltwater fluxes to determine the influence of each individually (Fig. 5 & Extended Data Fig. 6). Spatial outputs are shown as 30-year mean climatologies from 2090–2120 CE.

**Sea level model.** Sea level projections are calculated with the global sea-level model described in Ref.[79]. The model includes gravitational self-consistency, viscoelastic deformation of an elastically compressible solid Earth, changes in rotation of the Earth, migrating shorelines and inundation of water into areas free of (grounded) marine-based ice. Initial topography in the simulations is given by ETOPO1 globally and replaced by the initial bedrock elevation predicted beneath the Greenland and Antarctic ice sheets within each ice sheet model domain. Changes in ice thickness predicted with the Greenland and Antarctic ice sheet models are

combined into a global field, smoothed using a gaussian smoother and interpolated onto a global, gauss-legendre grid with 512 points in latitude and 1024 points in longitude. The interpolated grids are scaled to preserve total ice volume, and passed to the sea level model to compute sea level changes every 5 years with a resolution of up to spherical harmonic degree and order 512. Rheological structure of the solid Earth in the model varies radially. Elastic and density structure is taken from the Preliminary Reference Earth Model (PREM)[80], and viscosity structure is defined by a 120 km thick lithosphere and 100 km thick upper and lower mantle with viscosities of 5 x $10^{20}$ and 5 x $10^{21}$Pas, respectively. This viscosity model falls within a class of 1D viscosity profiles that are consistent with a wide range of global datasets related to ice-age glacial isostatic adjustment[81–83]. In the 100-year-long calculations presented here, however, the results are relatively insensitive to the choice of viscosity profile within the aforementioned class. Finally, computed sea level changes at 5 year intervals are normalized and scaled by the global average sea level values computed at the native resolution of the ice-sheet model.

**Experimental methods.** For both our model domains, we start our experimentation with a long spin-up procedure in which we take present-day input fields and allow our ice sheets to evolve under paleo-climate temperature forcings representing the last glacial cycle. The purpose of these simulations is to allow the thermal structure of the ice sheets to evolve over a sufficiently long period that even deep layers of the ice sheets are influenced by changing atmospheric conditions. We adopt a hierarchical grid refinement approach during this spin-up that includes a novel 'nudging' technique[84], such that when we incrementally increase the resolution of the model domains we also reset bed topography and ice thicknesses to present-day values. Specifically, our procedure for both model domains involves the following steps:

1. Initial smoothing run at 20 km (5 years Greenland, 20 years Antarctica)
2. Fixed geometry and climate, 20 km, 130,000 years
3. Evolving geometry and transient forcing of climate, 20 km resolution, from 130 ka BP to 5 ka BP
4. Topography updated to present-day, grid refined to 10 km, paleoclimate forcing from 4 ka BP to 1 ka BP
5. Topography and ice thickness updated to present-day, grid refined to 5 km, paleoclimate forcing from 1 ka BP to 0 ka BP
6. Topography and ice thickness updated to present-day, grid refined to 2.5 km for Greenland, 5 km for Antarctica, 500 year run under present climate.

The advantage of this approach is that it allows the thermal fields evolved during the long spin-up to be remapped back onto the present-day ice thickness fields, thereby both minimizing the mismatch at the end of the simulation between modelled and observed geometries,

and avoiding unintended smoothing of bedrock topography that occurs during the low resolution spin-up. By adopting multiple iterations of grid refinement and ice thickness nudging we ultimately complete the spin-up procedure with thermally and dynamically evolved, high resolution ice sheet simulations whose ice thicknesses and bed geometries are close to observed values (Extended Data Figures 7 & 8). Despite the broad agreement between modelled and observed values, there remain areas of mismatch, due to the 140 years of unconstrained evolution from 1860 to 2000. In Antarctica, one important area of mismatch is in the Amundsen Sea, where our simulation is thinner than observed, has slower than observed velocities in Pine Island Glacier, and faster than observed velocities in Thwaites Glacier. Although all of our sea-level-equivalent volume calculations are bias-corrected using a control run that also uses this initial state, we cannot rule out the possibility that modelled dynamics might differ if our present-day state were closer to observed values. It is not certain, however, that our initial state would necessarily promote grounding-line retreat, since experiments forced with regional climate and ocean model outputs led to a stabilization, or even advance, of the grounding line in this sector (see below). Clearly there is a delicate threshold in this sector which makes the ice sheet margin especially sensitive to ocean thermal forcing.

From these spun-up Greenland and Antarctic ice sheet models, we run forward experiments from 1860 to 2100 using full model physics and the CMIP5 climatologies described above for RCP 4.5 and 8.5. Although our ice sheets are well evolved, it is essential that they also correctly reproduce observed trends in recent mass changes. To that end, we undertake a manual procedure in which our simulations are repeatedly run at the full desired resolution (2.5 and 5 km) but with different parameterizations employed in each iteration. Whilst other studies have very effectively employed an ensemble approach[18,21], in which multiple parameter combinations are imposed and model validation is conducted on the final body of outputs, this would be computationally prohibitive for the high resolution simulations described here. Instead, we analyse each model run in turn, and make parameter adjustments based on the nature of any observed mismatch with empirical data. This approach results in simulations that fit multiple parameters not just at a single point in time, but over the periods of time for which observational constraints exist (Figure 1). Our tuning procedure for Greenland employs adjustments to both surface mass balance and basal sliding parameters in order to fit our simulations to observed trends. Our surface mass balance adjustment is based on previous studies (see main text), as is our basal sliding refinement. With the latter, however, we recognise that our approach is just one of the ways in which a fit to constraints might be achieved. Sensitivity tests illustrate the effect of applying a steeper sliding reduction, or none at all (Extended Data Figure 5**d**). Where no tapered reduction in basal traction is applied, net mass balance declines slightly (due to the reduction in refreezing) but is far too high to agree with observations (Extended Data Figure 5**d**, orange line). Doubling the reduction in basal traction used in our optimized scenario (blue line) results in a net mass balance trajectory that is only just in agreement with the observations, if published uncertainties are considered (Extended Data Figure 5**d**) light blue line). Rates of mass loss at 2100 CE are around 33% lower than the optimized scenario in the 'No taper' experiment, and 33% higher in the 'Steep taper' experiment. Future changes in basal sliding cannot be known,

so we are not able to fully constrain mass loss rates arising from dynamic processes such as these and this leads to uncertainty in our results. However, because dynamic thinning is fundamentally self-limiting[44,45] (by encouraging marine-terminating ice sheet margins to retreat onto land, where they tend to stabilise), our approach – targetting a central fit to the observational data – should reduce the errors in our projections as far as is possible, but we cannot rule out the possibility that mass loss rates by 2100 CE may be higher or lower than we predict. Higher resolution simulations than ours[85] may better resolve smaller outlet glaciers, and may perform better in this regard.

Once tuned in this manner, we then begin the following experimental procedure. We do not use fully coupled models. Instead, we first run a suite of ice sheet simulations under the two RCP scenarios and three stabilization scenarios described above. These simulations reveal the differences between emissions scenarios and stabilization times (Extended Data Figure 4), but do not incorporate ice–ocean–atmosphere feedbacks. To gauge the importance of such feedbacks we subsequently undertake new ice sheet simulations for RCP 4.5 and 8.5. To do this, we first take meltwater fluxes from the first iteration of our two ice sheets and add this as a surface freshwater flux to the oceans around the two ice sheets across a region adjacent to where the ice is lost (see 'Climate and ocean model' section above for definition of mask areas). For this we use the LOVECLIM intermediate complexity climate model described above. These LOVECLIM simulations from 2000 to 2100 CE evolve from a present-day equilibrium state and are perturbed only by the addition of meltwater. Thus, the differences in these simulations, compared to a control run in which no meltwater is added, are directly a consequence of the meltwater forcing. Whilst this approach may be simplistic, the consequences of adding the freshwater flux in our model are qualitatively similar to those produced with more sophisticated ocean models that allow melt input at depth[86,87] in that vertical mixing is reduced, leading to surface cooling and an associated expansion of sea ice. In fact, the depth at which meltwater is released appears to have little impact on modelled sea ice response[86]. However, we nonetheless recognise that the approximations inherent in this approach may mean that we do not fully resolve many of the finer-scale aspects of the oceanic response. Over seasonal to multi-annual timescales for example, fluctuations in the depth of the thermocline (which separates colder surface water from warmer subsurface water) occur[88–90]. These changes are driven by local oceanic and atmospheric conditions and are also known to influence basal melt rates, but currently only high-resolution limited domain ocean or coupled ocean–ice sheet models are able to capture such effects[46,89]. Similarly, our coarse-resolution ocean model most likely underrepresents advective heat transfer by meso-scale eddies[91,92], which play a critical role in transferring energy from the open ocean into continental shelf embayments such as the Weddell and Ross seas.

Acknowledging these simplifications, we take the outputs from our meltwater-perturbed climate model simulations and repeat our ice sheet simulations from 2000 to 2100 but add the air temperature, precipitation, and ocean temperature anomalies to our original CMIP5 climate forcings. This simple iteration aims to capture the influence of ice–ocean–atmosphere feedbacks on the ice sheet. The results of these simulations are shown in Figure 3. Since the meltwater feedback results in additional loss of ice from the two ice sheets, arising primarily from sub-

surface ocean warming, we re-run our LOVECLIM experiments for a second time but update the meltwater forcing to include the slight increase from the second ice sheet run. The 30-year averaged climate anomalies arising from this second iteration of the climate model are shown in Figure 4. Additional iterations of this process, or a tighter temporal coupling, might further refine the emergent climate anomalies by allowing feedback mechanisms (both positive and negative) to occur more quickly, but are computationally more demanding. To estimate meltwater-induced changes in climate variability, we calculate the standard deviation of climate fields from the detrended meltwater-forced runs, and difference century-end values from initial conditions. By then removing any background trend (calculated from our unforced control experiment) we derive a measure of how much our meltwater fluxes affect climate variability by the end of the century, compared to simulations in which such fluxes are omitted.

We also investigated the possible impact of driving our Antarctic ice sheet model with high-resolution regional climate[50] and ocean[72,93] model outputs, which directly provide melt fields for upper and lower ice sheet boundaries, respectively. Compared to our RCP 8.5 simulation using the CMIP5 climatology, our experiment forced with these regional models showed lower mass loss by 2100, and in fact showed grounding line advance of Amundsen Sea glaciers. This is not consistent with observational constraints, and likely arises from the fact that although the ice sheet model geometry is free to evolve, neither of the regional models used as inputs included an evolving ice sheet mask. Consequently, effects such as increased surface melt due to surface lowering (the 'elevation–melt feedback') are not captured, thereby allowing the glacier margin to thicken and stabilize over time, reducing the influence of oceanic melt. This result highlights the need for future regional modelling studies to incorporate evolving ice sheet geometries wherever possible.

For our sea level calculations, we take the ice geometry of our two ice sheets at five year intervals from the second iteration of the ice sheet model and add them to our sea-level model. The sea level model includes Earth rotation and deformation of a radially varying viscoelastic Earth model, and predicts a time-evolving gravitationally self-consistent spatial pattern of sea-level change through the 21st century. We run experiments in which we calculate the global fingerprints arising from ice sheet mass loss from each ice sheet individually, and combined. Outputs are scaled to the global mean sea level equivalent derived from our ice sheet model (Fig. 2**d**). The result of the combined ice sheet simulation is shown in Figure 4**d**. Whilst the global sea level model produces a self-consistent pattern of sea level rise, it does not capture the regional changes in sea surface height that arise from differential expansion of the water column arising from oceanic temperature changes. Taking the sea surface height anomaly (perturbed minus control experiment) from our climate simulations and adding this to our global sea level simulation yields a more complex pattern of sea level rise that primarily differs in the Southern Ocean where subsurface ocean warming is greatest (Fig. 4**h**).

**Code availability.** The Parallel Ice Sheet Model is freely available as open-source code from the PISM github repository (git://github.com/pism/pism.git). LOVECLIM is freely available for download from http://www.climate.be/modx/index.php?id=81. Figures were generated

using the Generic Mapping Tools[94]. Most figures use perceptually uniform colour palettes from the Scientific Colour Maps collection[95] and the CET Perceptually Uniform Colour Maps[96].

**Data availability.** CMIP5 data were downloaded from http://climexp.knmi.nl/. Antarctic bedrock topography and ice thickness data are from the BEDMAP2 compilation, available at http://www.antarctica.ac.uk//basresearch/ourresearch/az/bedmap2/. Greenland topography and ice thickness data are from BedMachine v3, available at https://nsidc.org/data/idbmg4. Greenland mass balance and geothermal heat flux data are available from the seaRISE website: http://websrv.cs.umt.edu/isis/index.php/Data. Information on Antarctic surface mass balance data is available at http://www.projects.science.uu.nl/iceclimate/models/antarctica.php#racmo23. Antarctic geothermal heat flux data are available at https://doi.pangaea.de/10.1594/PANGAEA.882503. Drainage basin outlines as shown in Figure 3 are based on ICESat data[97]. Antarctic grounding lines and calving lines shown in Figure 3**a** are from the MODIS-MOA 2009 dataset[98,99]. The datasets generated during and/or analysed during the current study are available from the corresponding author on reasonable request.


[52] Winkelmann, R., Martin, M. A., Haseloff, M., Albrecht, T., Bueler, E., Khroulev, C., and Levermann, A. The Potsdam Parallel Ice Sheet Model (PISM-PIK) - Part 1: Model description. *The Cryosphere* **5**, 715–726, August (2010).

[53] Aschwanden, A., Bueler, E., Khroulev, C., and Blatter, H. An enthalpy formulation for glaciers and ice sheets. *Journal of Glaciology* **58**, 441–457 (2012).

[54] Feldmann, J., Albrecht, T., Khroulev, C., Pattyn, F., and Levermann, A. Resolution-dependent performance of grounding line motion in a shallow model compared to a full-Stokes model according to the MISMIP3d intercomparison. *J. Glaciol.* **60**, 353–360 (2014).

[55] Golledge, N. R., Thomas, Z. A., Levy, R. H., Gasson, E. G. W., Naish, T. R., McKay, R. M., Kowalewski, D. E., and Fogwill, C. J. Antarctic climate and ice sheet configuration during a peak-warmth Early Pliocene interglacial. *Climate of the Past* **13**, 959975 (2017).

[56] Seroussi, H. and Morlighem, M. Representation of basal melting at the grounding line in ice flow models. *The Cryosphere Discussions* , https://doi.org/10.5194/tc–2018–117 (2018).

[57] Milillo, P., Rignot, E., Mouginot, J., Scheuchl, B., Morlighem, M., Li, X., and Salzer, J. T. On the short-term grounding zone dynamics of Pine Island Glacier, West Antarctica,

observed with COSMO-SkyMed interferometric data. *Geophysical Research Letters* **44**, 10436–10444 (2017).

[58] van den Broeke, M., Bus, C., Ettema, J., and Smeets, P. Temperature thresholds for degreeday modelling of Greenland ice sheet melt rates. *Geophysical Research Letters* **37**, L18501 (2010).

[59] Hellmer, H. and Olbers, D. A two-dimensional model for the thermohaline circulation under an ice shelf. *Antarctic Science* **1**, 325–336 (1989).

[60] Rignot, E. and Jacobs, S. S. Rapid bottom melting widespread near Antarctic Ice Sheet grounding lines. *Science* **296**, 2020–2023 (2002).

[61] Hellmer, H., Kauker, F., Timmermann, R., Determann, J., and Rae, J. Twenty-first-century warming of a large Antarctic ice-shelf cavity by a redirected coastal current. *Nature* **485**, 225–228 (2012).

[62] Levermann, A., Albrecht, T., Winkelmann, R., Martin, M. A., Haseloff, M., and Joughin, I. Kinematic first-order calving law implies potential for abrupt ice-shelf retreat. *The Cryosphere* **6**, 273–286 (2012).

[63] Fretwell, P., Pritchard, H. D., Vaughan, D. G., Bamber, J. L., Barrand, N. E., Bell, R., Bianchi, C., Bingham, R. G., Blankenship, D. D., Casassa, G., et al. Bedmap2: improved ice bed, surface and thickness datasets for Antarctica. *The Cryosphere* **7**(1), 375–393 (2013).

[64] Morlighem, M., Williams, C. N., Rignot, E., An, L., Arndt, J. E., Bamber, J. L., Catania, G., Chauché, N., Dowdeswell, J. A., Dorschel, B., et al. BedMachine v3: Complete bed topography and ocean bathymetry mapping of Greenland from multibeam echo sounding combined with mass conservation. *Geophysical Research Letters* **44**(21) (2017).

[65] Van Wessem, J., Reijmer, C., Morlighem, M., Mouginot, J., Rignot, E., Medley, B., Joughin, I., Wouters, B., Depoorter, M., Bamber, J., et al. Improved representation of East Antarctic surface mass balance in a regional atmospheric climate model. *Journal of Glaciology* **60**(222), 761–770 (2014).

[66] Ettema, J., van den Broeke, M. R., van Meijgaard, E., van de Berg, W. J., Bamber, J. L., Box, J. E., and Bales, R. C. Higher surface mass balance of the greenland ice sheet revealed by high-resolution climate modeling. *Geophysical Research Letters* **36**, JUN 16 (2009).

[67] Martos, Y. M., Catalán, M., Jordan, T. A., Golynsky, A., Golynsky, D., Eagles, G., and Vaughan, D. G. Heat flux distribution of Antarctica unveiled. *Geophysical Research Letters* **44**(22) (2017).

[68] Shapiro, N. and Ritzwoller, M. Inferring surface heat flux distributions guided by a global seismic model: Particular application to Antarctica. *Earth and Planetary Science Letters* **223**, 213–224 (2004).

[69] Sallée, J.-B., Shuckburgh, E., Bruneau, N., Meijers, A. J. S., Bracegirdle, T. J., Wang, Z., and Roy, T. Assessment of Southern Ocean water mass circulation and characteristics in CMIP5 models: Historical bias and forcing response. *Journal of Geophysical Research* **118**, 18301844 (2013).

[70] Turner, J., Bracegirdle, T. J., Phillips, T., Marshall, G. J., , and Hosking, J. S. An initial assessment of Antarctic sea ice extent in the CMIP5 models. *Journal of Climate* **26**, 14731484 (2013).

[71] Bracegirdle, T. J., Shuckburgh, E., Sallée, J.-B., Wang, Z., Meijers, A. J. S., Bruneau, N., Phillips, T., and Wilcox, L. J. Assessment of surface winds over the Atlantic, Indian, and Pacific Ocean sectors of the Southern Ocean in CMIP5 models: Historical bias, forcing response, and state dependence. *Journal of Geophysical Research* **118**, 547562 (2013).

[72] Naughten, K. A., Meisssner, K. J., Galton-Fenzi, B. K., England, M. H., Timmermann, R., and Hellmer, H. H. Future Projections of Antarctic Ice Shelf Melting Based on CMIP5 Scenarios. *Journal of Climate* **31**, 5243–5261 (2018).

[73] H., G., Brovkin, V., Fichefet, T., Haarsma, R., Jongma, J., Huybrechts, P., Mouchet, A., Selten, F., Barriat, P.-Y., Campin, J.-M., Deleersnijder, E., Driesschaert, E., Goelzer, H., Janssens, I., Loutre, M.-F., Maqueda, M. A. M., Opsteegh, T., Mathieu, P.-P., Munhoven, G., Petterson, E., Renssen, H., Roche, D. M., Schaeffer, M., Severijns, C., Tartinville, B., Timmermann, A., and Weber, N. Description of the Earth system model of intermediate complexity LOVECLIM version 1.2. *Geoscientific Model Development* **3**, 603633 (2010).

[74] Gent, P. R. and McWilliams, J. C. Isopycnal mixing in ocean circulation models. *Journal of Physical Oceanography* **20**(1), 150–155 (1990).

[75] Menviel, L., Timmermann, A., Timm, O. E., and Mouchet, A. Deconstructing the Last Glacial termination: the role of millennial and orbital-scale forcings. *Quaternary Science Reviews* **30**, 1155–1172 (2011).

[76] Abram, N. J., McGregor, H. V., Tierney, J. E., Evans, M. N., McKay, N. P., Kaufman, D. S., Thirumalai, K., Martrat, B., Goosse, H., Phipps, S. J., et al. Early onset of industrial-era warming across the oceans and continents. *Nature* **536**(7617), 411 (2016).

[77] Menviel, L., Spence, P., Yu, J., Chamberlain, M., Matear, R., Meissner, K., and England, M. Southern Hemisphere westerlies as a driver of the early deglacial atmospheric CO2 rise. *Nature Communications* **9**, DOI: 10.1038/s41467–018–04876–4 (2018).

[78] Randall, D. A., Wood, R. A., Bony, S., Colman, R., Fichefet, T., Fyfe, J., Kattsov, V., Pitman, A., Shukla, J., Srinivasan, J., et al. Climate models and their evaluation. In *Climate change 2007: The physical science basis. Contribution of Working Group I to the Fourth Assessment Report of the IPCC (FAR)*, 589–662. (2007).

[79] Gomez, N., Mitrovica, J. X., Huybers, P., and Clark, P. U. Sea level as a stabilizing factor for marine-ice-sheet grounding lines. *Nature Geoscience* **3**, 850–853 (2010).

[80] Dziewonski, A. M. and Anderson, D. L. Preliminary reference Earth model. *Phys. Earth Planet. Inter.* **25**, 297356 (1981).

[81] Lambeck, K., Smither, C., and Ekman, M. Tests of glacial rebound models for fennoscandinavia based on instrumented sea- and lake-level records. *Geophysical Journal International* **135**(2), 375–387 (1998a).

[82] Mitrovica, J. X. and Forte, A. M. A new inference of mantle viscosity based upon joint inversion of convection and glacial isostatic adjustment data. *Earth and Planetary Science Letters* **225**, 177–189 (2004).

[83] Lambeck, K., Rouby, H., Purcell, A., Sun, Y., and Sambridge, M. Sea level and global ice volumes from the Last Glacial Maximum to the Holocene. *Proceedings of the National Academy of Sciences* **111**, 1529615303 (2014).

[84] Stuhne, G. and Peltier, W. Reconciling the ICE-6G_C reconstruction of glacial chronology with ice sheet dynamics: The cases of Greenland and Antarctica. *Journal of Geophysical Research* **120**(9), 1841–1865 (2015).

[85] Aschwanden, A., Fahnestock, M. A., and Truffer, M. Complex Greenland outlet glacier flow captured. *Nature Communications* **7**, 10524 (2016).

[86] Pauling, A. G., Bitz, C. M., Smith, I. J., and Langhorne, P. J. The response of the Southern Ocean and Antarctic sea ice to freshwater from ice shelves in an Earth system model. *Journal of Climate* **29**(5), 1655–1672 (2016).

[87] Merino, N., Jourdain, N. C., Le Sommer, J., Goosse, H., Mathiot, P., and Durand, G. Impact of increasing Antarctic glacial freshwater release on regional sea-ice cover in the Southern Ocean. *Ocean Modelling* **121**, 76–89 (2018).

[88] Dong, S., Sprintall, J., Gille, S. T., and Talley, L. Southern Ocean mixed-layer depth from Argo float profiles. *Journal of Geophysical Research: Oceans* **113**, C06013 (2008).

[89] Dutrieux, P., De Rydt, J., Jenkins, A., Holland, P. R., Ha, H. K., Lee, S. H., Steig, E. J., Ding, Q., Abrahamsen, E. P., and Schröder, M. Strong sensitivity of Pine Island ice-shelf melting to climatic variability. *Science* **343**(6167), 174–178 (2014).

[90] Webber, B. G., Heywood, K. J., Stevens, D. P., Dutrieux, P., Abrahamsen, E. P., Jenkins, A., Jacobs, S. S., Ha, H. K., Lee, S. H., and Kim, T. W. Mechanisms driving variability in the ocean forcing of Pine Island Glacier. *Nature Communications* **8**, 14507 (2017).

[91] Thompson, A. F., Heywood, K. J., Schmidtko, S., and Stewart, A. L. Eddy transport as a key component of the Antarctic overturning circulation. *Nature Geoscience* **7**, 879–884 (2014).

[92] Stewart, A. L. and Thompson, A. F. Eddy-mediated transport of warm Circumpolar Deep Water across the Antarctic Shelf Break. *Geophysical Research Letters* **42**(2), 432–440 (2015).

[93] Naughten, K. A., Meissner, K. J., Galton-Fenzi, B. K., England, M. H., Timmermann, R., Hellmer, H. H., Hattermann, T., and Debernard, J. B. Intercomparison of Antarctic ice-shelf, ocean, and sea-ice interactions simulated by MetROMS-iceshelf and FESOM 1.4. *Geoscientific Model Development* **11**, 1257–1292 (2018).

[94] Wessel, P., Smith, W. H., Scharroo, R., Luis, J., and Wobbe, F. Generic mapping tools: improved version released. *Eos, Transactions American Geophysical Union* **94**, 409–410 (2013).

[95] Crameri, F. Geodynamic diagnostics, scientific visualisation and StagLab 3.0. *Geoscientific Model Development* **11**, 2541–2562 (2018).

[96] Kovesi, P. Good Colour Maps: How to Design Them. *CoRR* **abs/1509.03700** (2015).

[97] Zwally, H. J., Giovinetto, M. B., Beckley, M. A., and Saba, J. L. Antarctic and Greenland Drainage Systems. *GSFC Cryospheric Sciences Laboratory* , http://icesat4.gsfc.nasa.gov/cryo_data/ant_grn_drainage_systems.php (2012).

[98] Scambos, T. A., Haran, T. M., Fahnestock, M. A., Painter, T. H., and Bohlander, J. Modis-based mosaic of antarctica (moa) data sets: Continent-wide surface morphology and snow grain size. *Remote Sensing of Environment* **111**(2), 242–257 (2007).

[99] Haran, T., Bohlander, J., Scambos, T., Painter, T., and Fahnestock, M. MODIS Mosaic of Antarctica 2008-2009 (MOA2009) Image Map. *National Snow and Ice Data Center* **http://dx.doi.org/10.7265/N5KP8037**, digital media (2014).

[100] Rignot, E., Bamber, J. L., van den Broeke, M. R., Davis, C., Li, Y., van de Berg, W. J., and van Meijgaard. Recent antarctic ice mass loss from radar interferometry and regional climate modelling. *Nature Geoscience* **1**, doi:10.1038/ngeo102 (2008).

[101] Rignot, E., Box, J. E., Burgess, E., and Hanna, E. Mass balance of the greenland ice sheet from 1958 to 2007. *Geophys. Res. Lett.* **35** (2008).

[102] King, M. A., Bingham, R. J., Moore, P., Whitehouse, P. L., Bentley, M. J., and Milne, G. A. Lower satellite-gravimetry estimates of Antarctic sea-level contribution. *Nature* **491**, 586–589 (2012).

[103] Lenaerts, J., van den Broeke, M., van de Berg, W., van Meijgaard, E., and Munneke, P. A new, high-resolution surface mass balance map of Antarctica (1979–2010) based on regional atmospheric climate modeling. *Geophysical Research Letters* **39**, L04501 (2012).

[104] Rignot, E., Jacobs, S., Mouginot, J., and Scheuchl, B. Ice-shelf melting around Antarctica. *Science* **341**, 266270 (2013).

[105] Liu, Y., Moore, J. C., Cheng, X., Gladstone, R. M., Bassis, J. N., Liu, H., Wen, J., and Hui, F. Ocean-driven thinning enhances iceberg calving and retreat of Antarctic ice shelves. *Proceedings of the National Academy of Sciences* **112**, 3263–3268 (2015).

[106] Depoorter, M. A., Bamber, J. L., Griggs, J. A., Lenaerts, J. T. M., Ligtenberg, S. R. M., van den Broeke, M. R., and Moholdt, G. Calving fluxes and basal melt rates of Antarctic ice shelves. *Nature* **502**, 89–92 (2013).

[107] Shepherd, A., Ivins, E. R., Geruo, A., Barletta, V. R., Bentley, M. J., Bettadpur, S., Briggs, K. H., Bromwich, D. H., Forsberg, R., Galin, N., et al. A reconciled estimate of ice-sheet mass balance. *Science* **338**(6111), 1183–1189 (2012).

[108] Rignot, E. and Kanagaratnam, P. Changes in the velocity structure of the greenland ice sheet. *Science* **311**, 986–990 (2006).

[109] Box, J. E., Bromwich, D. H., and Bai, L. S. Greenland ice sheet surface mass balance 1991-2000: Application of polar mm5 mesoscale model and in situ data. *JOURNAL OF GEOPHYSICAL RESEARCH-ATMOSPHERES* **109**(D16), AUG 26 (2004).

[110] Sasgen, I., van den Broeke, M., Bamber, J. L., Rignot, E., Sørensen, L. S., Wouters, B., Martinec, Z., Velicogna, I., and Simonsen, S. B. Timing and origin of recent regional ice-mass loss in Greenland. *Earth and Planetary Science Letters* **333**, 293–303 (2012).

[111] Helm, V., Humbert, A., and Miller, H. Elevation and elevation change of Greenland and Antarctica derived from CryoSat-2. *The Cryosphere* **8**(4), 1539–1559 (2014).

[112] Martín-Español, A., Zammit-Mangion, A., Clarke, P. J., Flament, T., Helm, V., King, M. A., Luthcke, S. B., Petrie, E., Rémy, F., Schön, N., et al. Spatial and temporal Antarctic Ice Sheet mass trends, glacio-isostatic adjustment, and surface processes from a joint inversion of satellite altimeter, gravity, and GPS data. *Journal of Geophysical Research* **121**(2), 182–200 (2016).

[113] Gardner, A. S., Moholdt, G., Scambos, T., Fahnstock, M., Ligtenberg, S., van den Broeke, M., and Nilsson, J. Increased West Antarctic and unchanged East Antarctic ice discharge over the last 7 years. *The Cryosphere* **12**(2), 521–547 (2018).

[114] McMillan, M., Shepherd, A., Sundal, A., Briggs, K., Muir, A., Ridout, A., Hogg, A., and Wingham, D. Increased ice losses from Antarctica detected by CryoSat-2. *Geophysical Research Letters* **41**(11), 3899–3905 (2014).

[115] Turner, J., Connolley, W. M., Leonard, S., Marshall, G. J., and Vaughan, D. G. Spatial and temporal variability of net snow accumulation over the Antarctic from ECMWF reanalysis project data. *International Journal of Climatology* **19**(7), 697–724 (1999).

[116] Velicogna, I. and Wahr, J. Time-variable gravity observations of ice sheet mass balance: Precision and limitations of the GRACE satellite data. *Geophysical Research Letters* **40**(12), 3055–3063 (2013).

[117] Van de Berg, W., Van den Broeke, M., Reijmer, C., and Van Meijgaard, E. Reassessment of the Antarctic surface mass balance using calibrated output of a regional atmospheric climate model. *Journal of Geophysical Research* **111**(D11) (2006).

[118] Wilson, N. J., Straneo, F., and Heimbach, P. Satellite-derived submarine melt rates and mass balance (2011–2015) for Greenland's largest remaining ice tongues. *The Cryosphere* **11**, 2773–2782 (2017).

[119] Bigg, G. R., Wei, H.-L., Wilton, D. J., Zhao, Y., Billings, S. A., Hanna, E., and Kadirkamanathan, V. A century of variation in the dependence of Greenland iceberg calving on ice sheet surface mass balance and regional climate change. *Proceedings of the Royal Society, A* **470**(2166), 20130662 (2014).

[120] Nagler, T., Rott, H., Hetzenecker, M., Wuite, J., and Potin, P. The Sentinel-1 mission: New opportunities for ice sheet observations. *Remote Sensing* **7**(7), 9371–9389 (2015).

[121] Rignot, E., Mouginot, J., and Scheuchl, B. Ice Flow of the Antarctic Ice Sheet. *Science* **333**, 1427–1430 (2011).

# Extended Data

**Extended Data Table 1 | Empirical constraints used to guide Antarctic ice sheet parameterization.** Estimates of changes in total mass, surface mass balance (SMB), sub-ice shelf melt (BMB), and iceberg calving from recent satellite-based studies, including uncertainties. Data provide targets for ice sheet simulations shown in Fig. 1.

**Antarctica**

| | | Period | Rate (Gt / yr) | Uncertainty (± Gt /yr) |
|---|---|---|---|---|
| **Total mass** | Bamber et al. (2018) | 1992-1997 | -27 | 106 |
| | | 1997-2002 | -103 | 106 |
| | | 2002-2007 | -25 | 54 |
| | | 2007-2012 | -117 | 28 |
| | | 2012-2017 | -191 | 47 |
| | Gardner et al. (2018) | 2008-2015 | -183 | 94 |
| | Shepherd et al. (2018) | 1992-1997 | -49 | 67 |
| | | 1997-2002 | -38 | 64 |
| | | 2002-2007 | -73 | 53 |
| | | 2007-2012 | -160 | 50 |
| | | 2012-2017 | -219 | 43 |
| | Martin-Espanol et al. (2016) | 2010-2013 | -159 | 22 |
| | Helm et al. (2014) | 2011-2014 | -116 | 76 |
| | McMillan et al. (2014) | 2010-2013 | -159 | 48 |
| | Velicogna & Wahr (2013) | 2003-2011 | -118 | 66 |
| | King et al. (2012) | 2002-2010 | -69 | 18 |
| | Rignot et al. (2008) | 1995-1996 | -112 | 91 |
| | | 1999-2000 | -138 | 92 |
| | | 2005-2006 | -196 | 92 |
| **SMB** | Lenaerts et al. (2012) | 1979-2010 | 2418 | 181 |
| | Rignot et al. (2008) | 1999-2000 | 2055 | 122 |
| | van der Berg et al. (2006) | 1980-2004 | 2521 | 33 |
| | Turner et al. (1999) | 1979-1993 | 2106 | 299 |
| **BMB** | Liu et al. (2015) | 2005-2011 | 1516 | 106 |
| | Depoorter et al. (2013) | 1995-2009 | 1454 | 174 |
| | Rignot et al. (2013) | 2003-2008 | 1325 | 235 |
| **Calving** | Liu et al. (2015) | 2005-2011 | 755 | 25 |
| | Depoorter et al. (2013) | 1995-2009 | 1321 | 144 |
| | Rignot et al. (2013) | 2003-2008 | 1089 | 139 |

**Extended Data Table 2 | Empirical constraints used to guide Greenland ice sheet parameterization.** Estimates of changes in total mass, surface mass balance (SMB), sub-ice shelf melt (BMB), and iceberg calving from recent satellite-based and modelling studies, including uncertainties. Data provide targets for ice sheet simulations shown in Fig. 1.

**Greenland**

| | | Period | Rate (Gt / yr) | Uncertainty (± Gt /yr) |
|---|---|---|---|---|
| **Total mass** | Bamber et al. (2018) | 1992-1997 | 31 | 83 |
| | | 1997-2002 | -47 | 81 |
| | | 2002-2007 | -206 | 28 |
| | | 2007-2012 | -320 | 10 |
| | | 2012-2017 | -247 | 15 |
| | Forsberg et al. (2017) | 2002-2015 | -264 | 25 |
| | Velicogna & Wahr (2013) | 2003-2012 | -265 | 40 |
| | Sasgen et al. (2012) | 2003-2009 | -265 | 58 |
| | Shepherd et al. (2012) | 1992-2000 | -51 | 65 |
| | | 1993-2003 | -83 | 63 |
| | | 2000-2011 | -211 | 37 |
| | Rignot et al. (2008) GRL | 1957-1958 | -119 | 68 |
| | | 1963-1964 | -106 | 73 |
| | | 1995-1996 | -97 | 47 |
| | Rignot & Kanagaratnam (2006) | 2005-2006 | -210 | 40 |
| **SMB** | Rignot et al. (2008) GRL | 1957-1958 | 272 | 41 |
| | | 1963-1964 | 299 | 45 |
| | | 1995-1996 | 300 | 45 |
| | | 1999-2000 | 277 | 42 |
| | | 2003-2004 | 242 | 36 |
| | | 2004-2005 | 233 | 35 |
| | | 2005-2006 | 234 | 35 |
| | | 2006-2007 | 228 | 34 |
| | Box & Bromwich (2004) | 1992-1998 | 193 | 179.5 |
| **BMB** | Wilson et al. (2017) | 2011-2015 | 23.7 | 3.2 |
| **Calving** | Bigg et al. (2014) | 1900-1910 | 250 | 204 |
| | | 1910-1920 | 216 | 185 |
| | | 1920-1930 | 264 | 209 |
| | | 1930-1940 | 267 | 172 |
| | | 1940-1950 | 211 | 228 |
| | | 1950-1960 | 148 | 187 |
| | | 1960-1970 | 96 | 85 |
| | | 1970-1980 | 254 | 340 |
| | | 1980-1990 | 335 | 407 |
| | | 1990-2000 | 659 | 345 |
| | | 2000-2009 | 271 | 238 |

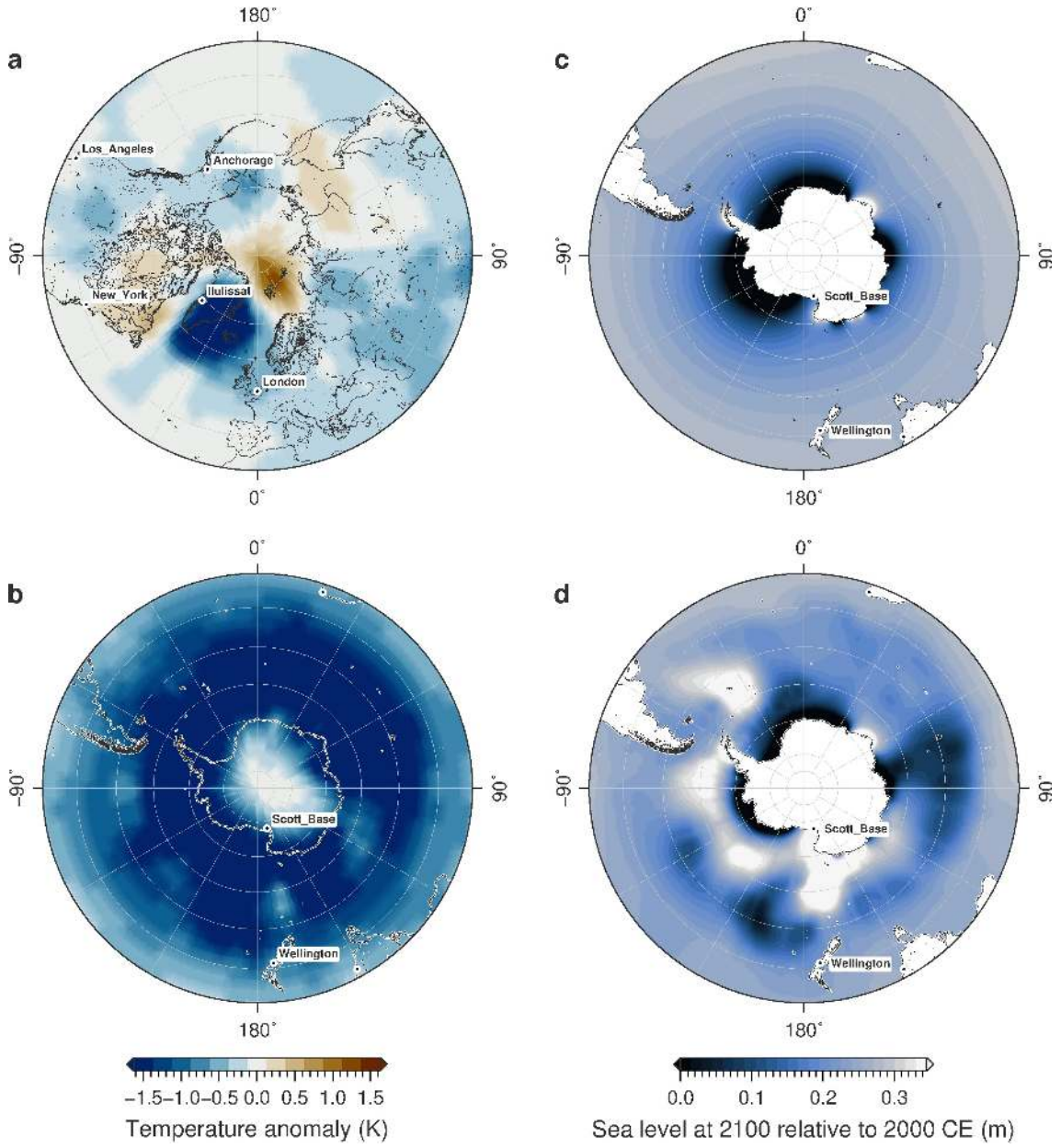


**Extended Data Figure 1 | High-latitude air temperature and sea-level anomalies.** Air (surface) temperature anomalies at 2100 CE arising from meltwater perturbations from ice sheets simulated under an RCP 8.5 climate scenario. Arctic landmasses experience slight cool or warm anomalies **a,** but temperatures over the Arctic ocean warm significantly in the region to the northeast of Greenland (around Svalbard), as far north as the North Pole. In the Southern Hemisphere **b,** cooling of up to 3–4°C occurs across the Southern Ocean and around the margins of Antarctica. Temperature anomalies are 30-year means to avoid aliasing short-term variability. Sea level changes in the Southern Ocean and around Antarctica **c,** computed from the sea level model, and **d,** with the addition of sea surface height changes arising from ocean temperature changes. The calculated thermosteric anomalies are from a 30-year mean in order to avoid aliasing short-term variability.

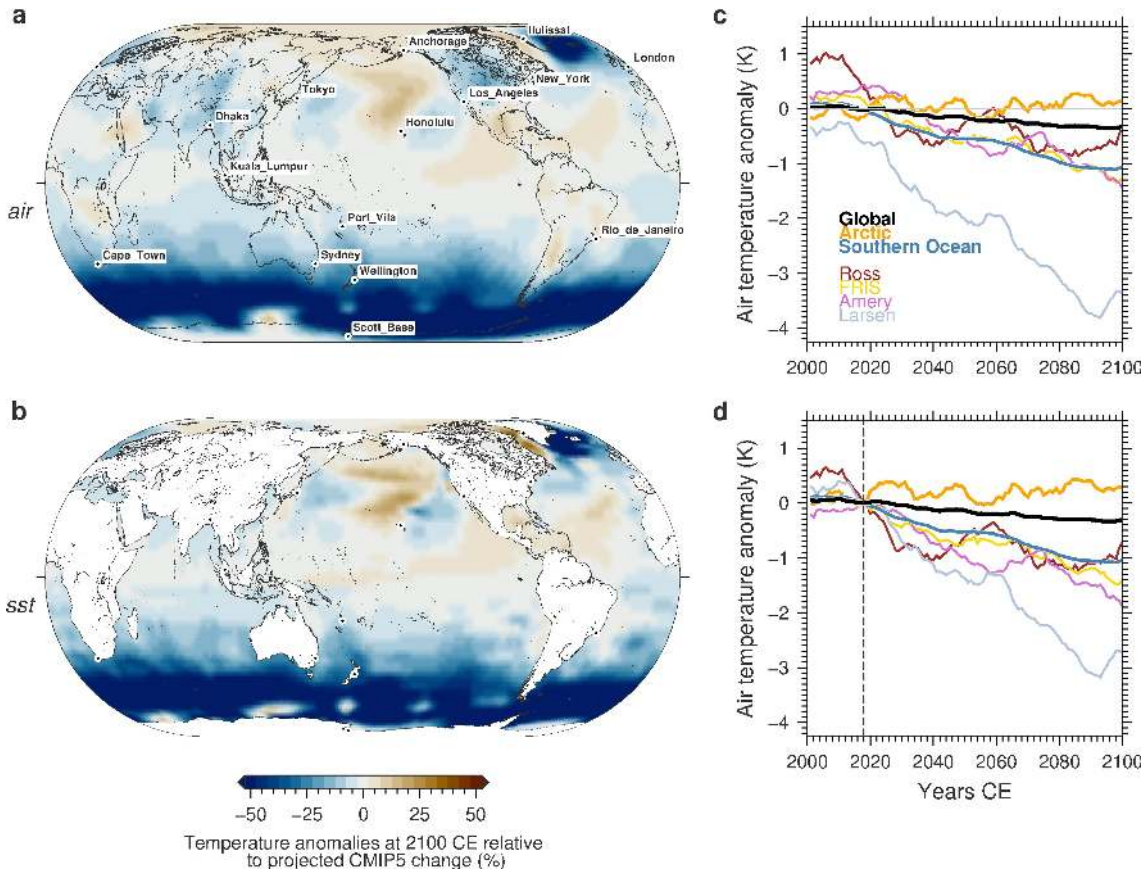


**Extended Data Figure 2 | Global and regional surface temperature anomalies.** Surface **a,** air and **b,** sea surface temperature anomalies at 2100 CE arising solely from imposed meltwater fluxes, as a percentage of CMIP5 predictions based on emissions forcing but not including meltwater fluxes. **c,** Zonally and meridionally averaged surface air temperature anomalies for the globe, the Southern Ocean (40-85°S), and over the four largest ice shelves in Antarctica. **d,** Same as **c,** but adjusted to give changes relative to 2018.

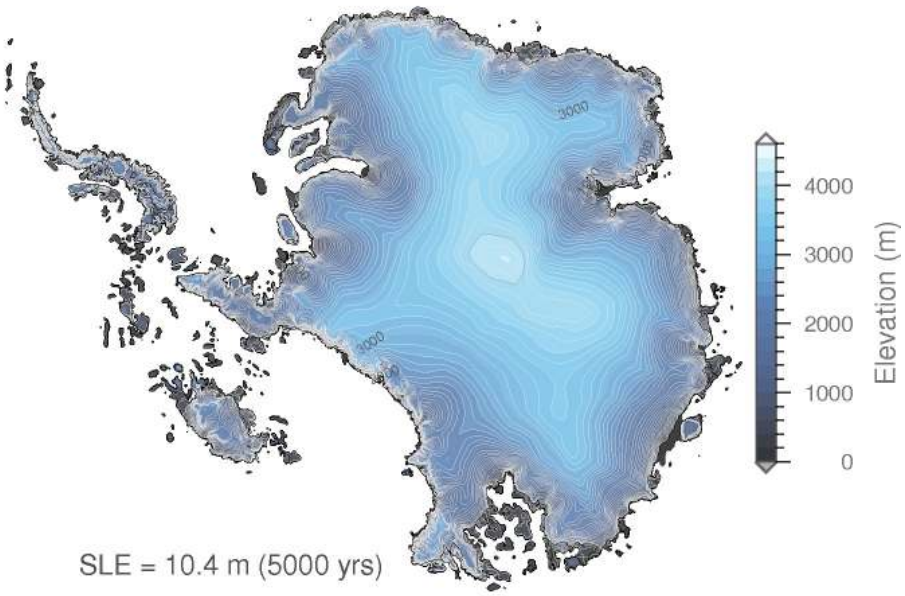


**Extended Data Figure 3 | Antarctic ice sheet extent under Pliocene conditions.** Five-kilometer resolution simulation of the Antarctic ice sheet under peak warmth Pliocene conditions, based on proxy-constrained climate and ocean fields from regional climate modelling[55] but employing an identical ice sheet parameterisation to that used for the RCP simulations presented in the main paper. The total sea-level equivalent mass loss after 5000 years is 10.4 m, close to the 11.3 m simulated by a previous study that employed ice shelf hydrofracture and marine ice cliff instability[21], neither of which are used here.

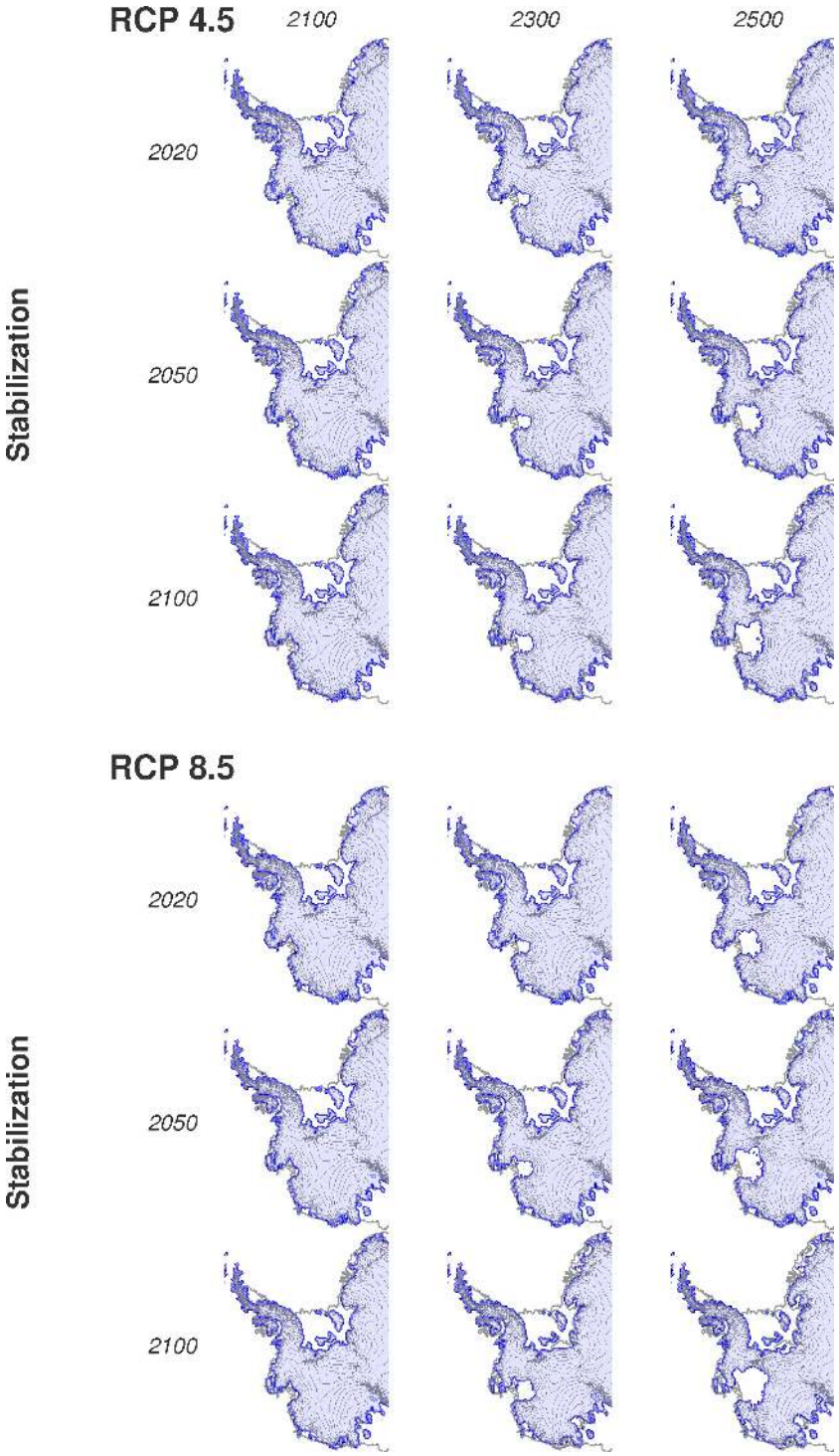


**Extended Data Figure 4 | Committed response of West Antarctica.** Extent of grounded ice in West Antarctica at 2100, 2300, 2500 CE for two emissions pathways and experiments in which the climate forcing is held constant from either 2020, 2050, or 2100, but without the inclusion of ice–ocean–atmosphere feedbacks. Mass loss in these scenarios illustrates long-term commitments locked in by cumulative forcing up to the point of stabilization. Note that Thwaites Glacier basin retreats in all scenarios, suggesting that the threshold for its stability has already been passed. Contour intervals are 250 m. Black lines show modern coast, for context.

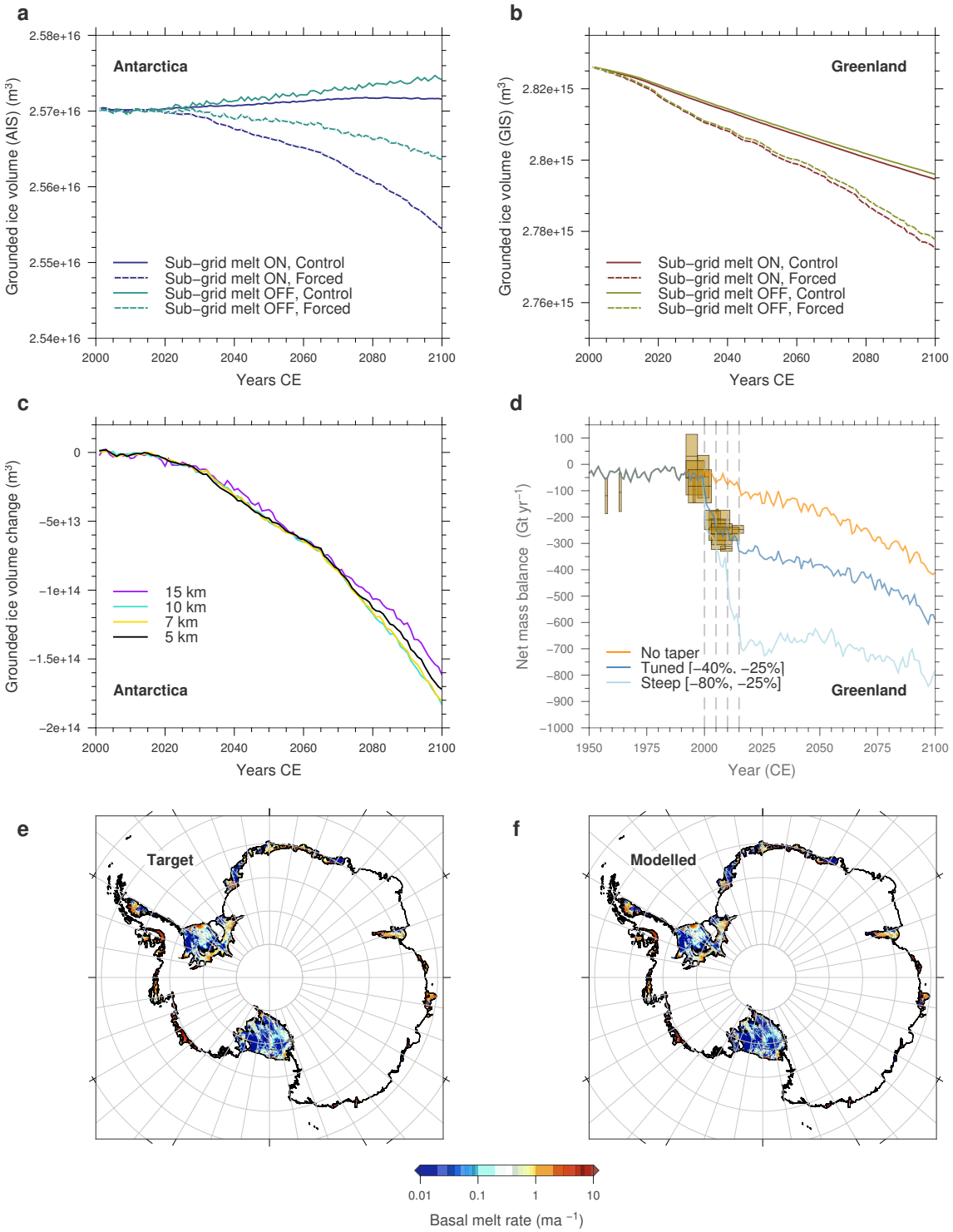


**Extended Data Figure 5 | Grounding line sensitivity and basal melt parameterisation.** Control run (constant Year-2000 climatology) and RCP 8.5-forced experiments (including

ice–ocean–atmosphere feedbacks) for **a,** Antarctica and **b,** Greenland, both with and without the incorporation of the sub-grid grounding line melt scheme. Without the scheme, Antarctic ice volumes are higher in the forced run than with sub-grid melt enabled, but the control run also increases in volume suggesting that other aspects of model parameterisation would need to be optimised to ensure agreement with observational constraints (Extended Data Tables 1 & 2). Greenland simulations are far less affected by the sub-grid melt scheme. Note that the Greenland runs shown all incorporate the evolving surface mass balance and basal traction parameterisation (see 'Methods'), for clearer comparison between control and perturbed experiments. **c,** Grounded ice volume change in Antarctica, compared to control runs, simulated by our ice sheet model using a range of horizontal grid resolutions but otherwise identical parameterisation and including the sub-grid grounding line basal melt scheme. **d,** Rate of Greenland ice sheet mass loss for the 'best-fit' simulation (dark blue line) compared to simulations in which either a steeper increase in sliding is applied (light blue line), or sliding is maintained at a constant value for the entire run (orange line). Numbers in square braces quantify the change in till friction angle in the piecewise linear basal traction parameter below -200 m and above 500 m, relative to the 'No taper' experiment. Gold boxes show the time span ($x$ axis) and uncertainty ($y$ axis) of empirical data values used as targets during parameter optimisation, from sources detailed in Extended Data Tables 1 & 2. **e,** Target melt rates from an empirically-constrained[104,106] ice sheet simulation[26] are used as inputs to an inverse scheme that solves for a spatially distributed melt factor to translate CMIP5 sea surface temperatures into **f,** realistic melt fields. This approach dramatically improves the representation of ice shelf basal melting in our simulation compared to previous studies[19,21].

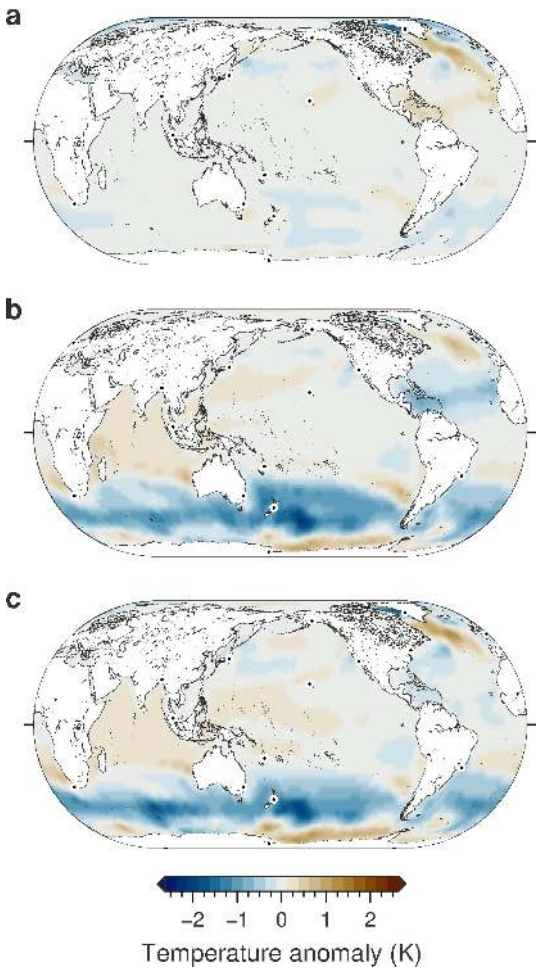


**Extended Data Figure 6 | Ice sheet influence on subsurface ocean temperature.** Ocean temperature anomalies by 2100 at 415 m depth from **a,** Greenland meltwater flux only, **b,** Antarctic meltwater flux only, and **c,** combined meltwater flux from both ice sheets. Anomalies are 30-year means to avoid aliasing short-term variability.

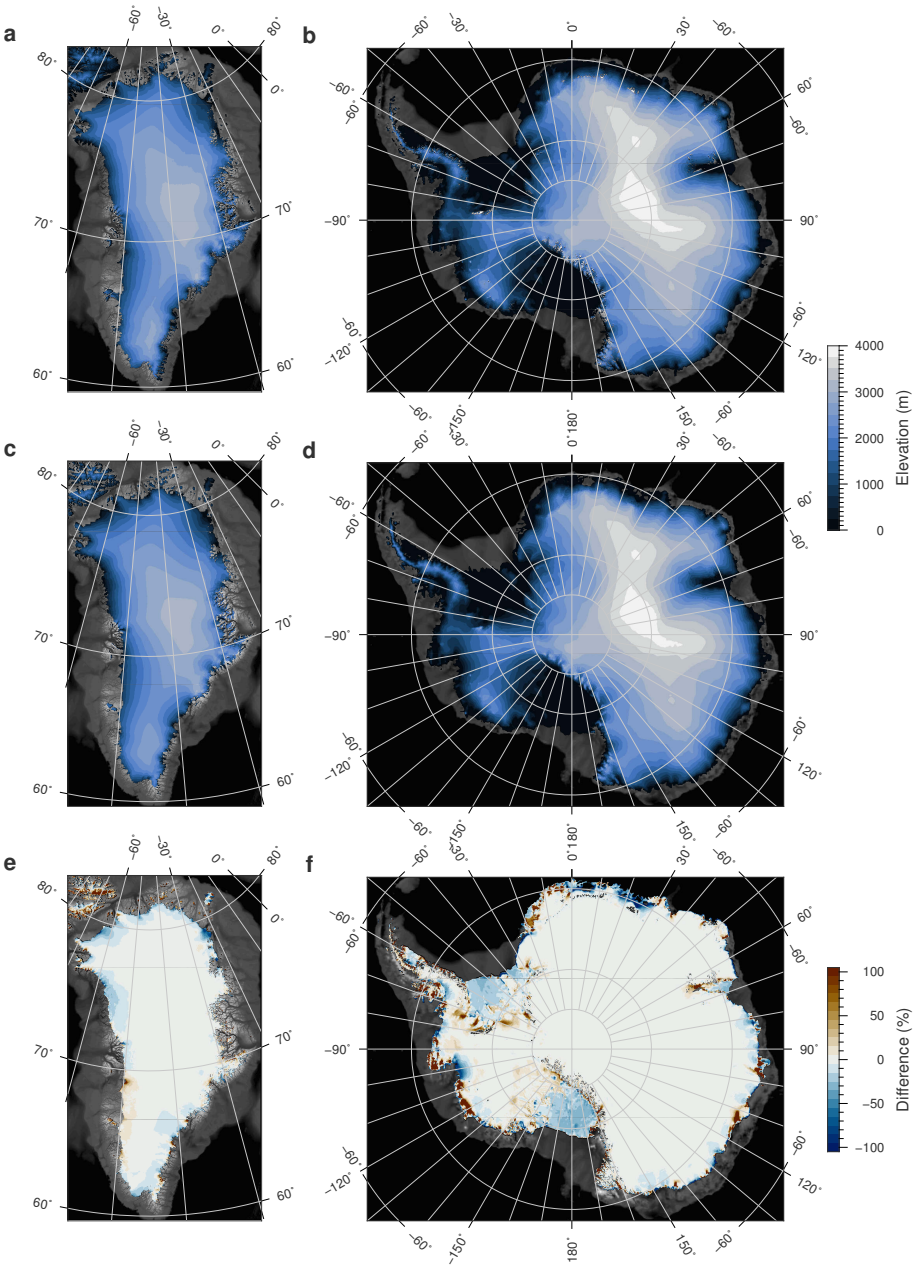


**Extended Data Figure 7 | Modelled versus measured surface elevation.** Measured values of surface elevation of the **a,** Greenland[64] and **b,** Antarctic[63] ice sheets compared to modelled values **(c, d)** at year 2000. Differences between the two (modelled minus observed) are shown in lowermost panels **(e, f)**.

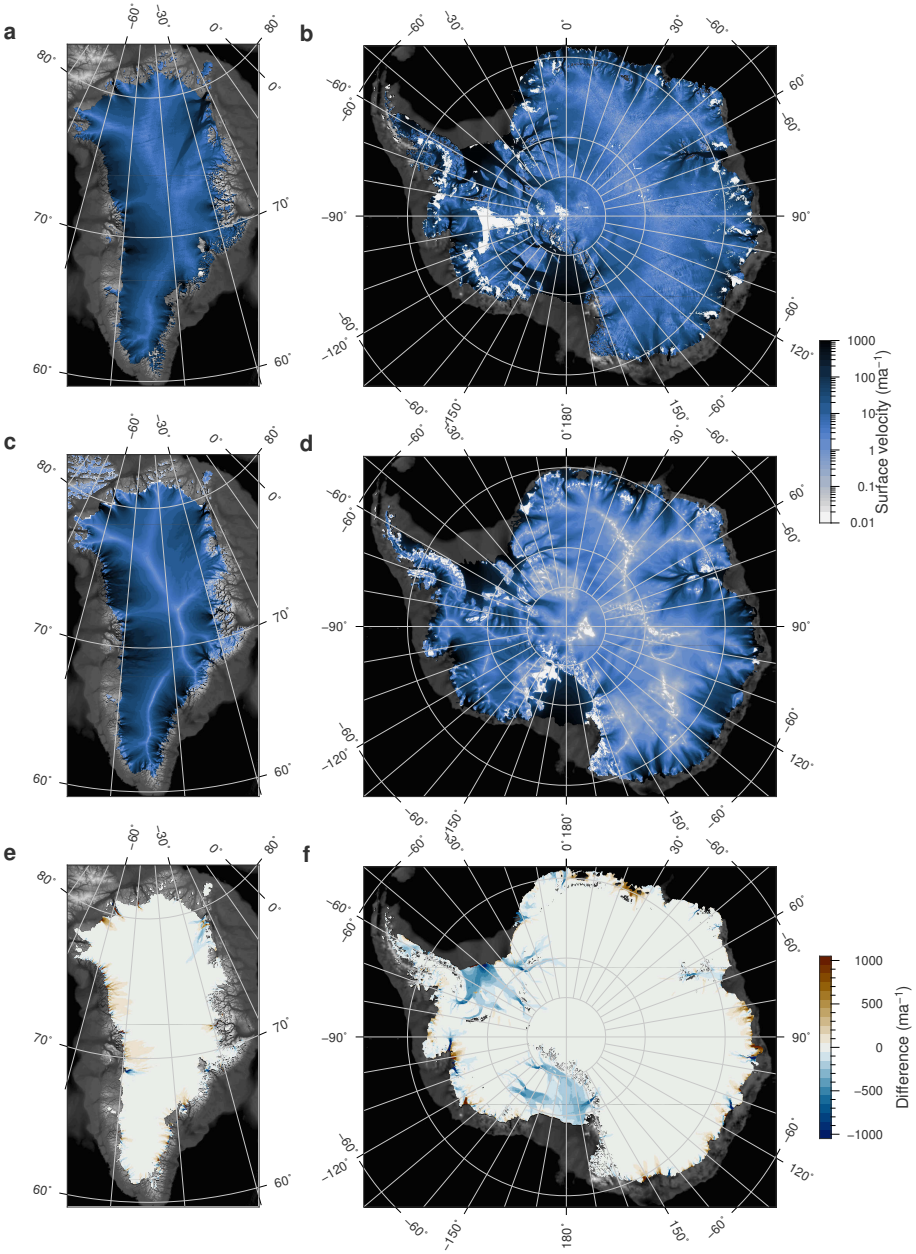


**Extended Data Figure 8 | Modelled versus measured surface velocity.** Measured values of surface velocity of the **a,** Greenland[120] and **b,** Antarctic[121] ice sheets compared to modelled values **(c, d)** at year 2000. Differences between the two (modelled minus observed) are shown in lowermost panels **(e, f)**.